Dual Shapiro steps of a phase-slip junction in the presence of a parasitic capacitance

master's thesis

Submitted to the Faculty of Mathematics, Computer Science and Natural Sciences at RWTH Aachen University

presented by

Lisa Arndt

under the supervision of

Prof. Dr. Fabian Hassler

and

Prof. Dr. David DiVincenzo

JARA-Institute for Quantum Information

05/2018

Abstract

This thesis investigates the emergence of dual Shapiro steps in the IV-curve of a single Josephson junction in the phase-slip regime. In particular, we analyze the detrimental effect of the parasitic capacitance between the biasing lines and how it can be remedied by an on-chip superinductance. We obtain an explicit analytical expression for the height of dual Shapiro steps as a function of the ratio of the parasitic capacitance to the superinductance. Using this result, we provide a quantitative estimate of the dual Shapiro step height. Our calculations reveal that even in the presence of a parasitic capacitance it should be possible to observe dual Shapiro steps with realistic experimental parameters.

Contents

List of Figures

Chapter 1

Introduction

1.1 Introduction and chapter overview

This thesis deals with the topic of Bloch oscillations in small Josephson junctions. First proposed in 1985 [1], these Bloch oscillations have important applications in metrology since their frequency is proportional to the current flowing through the junction. Indeed, they could provide the last link between current and frequency needed to close the quantum metrology triangle [2] shown in Fig. 1.1. The completion of this triangle would allow a self-consistent definition of voltage, current and frequency in terms of fundamental constants.

In order to observe Bloch oscillations, the Josephson junction needs to be operated in the phase-slip regime, where the Josephson junction effectively realizes a phase-slip junction [3]. The voltage drop V_P across a phase-slip junction depends on the charge Q flowing through the junction via $V_P = V_c \sin(\pi Q/e)$, with V_c the critical voltage of the phase-slip junction. It is clear that a constant current, $Q = I_0 t$, flowing through the junction causes an oscillating voltage — the so-called Bloch oscillation — with frequency $\omega_B = \pi I_0/e$. These oscillations can be measured by introducing an additional, small AC-drive. Inserting the resulting charge dynamic, $Q = I_0 t - I_{\mathrm{ac}} \cos(\omega_0 t)/\omega_0$, into the voltage relation of the phase-slip junction leads to voltage steps at constant current in the IV-curve. These steps occur when the Bloch oscillation frequency ω_B is an integer multiple of the drive frequency ω_0. Then, the incident radiation phase-locks with the Bloch oscillations in the junction resulting in dual Shapiro steps at constant current $I_0 = ne\omega_0/\pi,\ n \in \mathbb{Z} \setminus \{0\}$.

However, first attempts to demonstrate dual Shapiro steps [4, 5] did not reveal clear current steps in the IV-curve. Unlike conventional Shapiro steps, a

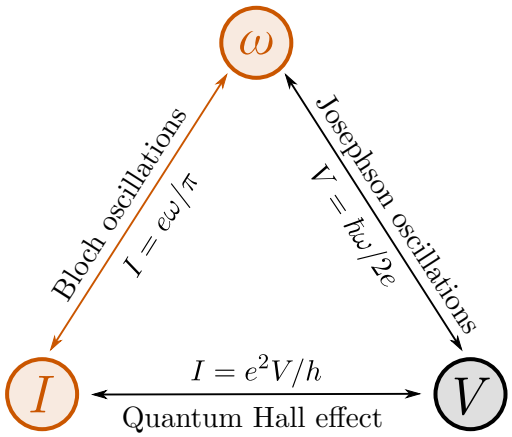

Figure 1.1: Quantum metrology triangle [2] between voltage, current, and frequency. Josephson oscillations and quantum Hall effect link constant voltage to frequency and current, respectively. The last needed link between current and frequency could be provided by Bloch oscillations via the observation of dual Shapiro steps. The completion of this triangle would allow a self-consistent definition of voltage, current and frequency in terms of fundamental constants of nature.

measurement of dual Shapiro steps is impeded by the presence of a parasitic capacitance between the biasing lines [6]. This capacitance shunts the junction, suppressing the amplitude of the Bloch oscillation. It is known that the detrimental effect of the parasitic capacitance can be remedied by an on-chip superinductance [6]. However, there has not been a theoretical study on the quantitative influence of the parasitic capacitance on the dual Shapiro step height in presence of the superinductance.

In this thesis, we combine an on-chip superinductance, screening the parasitic capacitance, with a large off-chip resistance, dissipating the excess energy. For this setup, we provide analytical results for the height of the dual Shapiro steps and verify our findings using numerical simulations. Hopefully, our predictions can help to advance the current experimental efforts towards observing dual Shapiro steps.

This thesis is organized as follows. In Ch. 2, we introduce the concept of phase-slip junctions and discuss the conditions necessary to turn a Josephson junction into such a phase-slip junction. Next, we use an ideal, simplified model of a phase-slip junction in series with a large resistance and voltage source to study the emergence of Bloch oscillations and dual Shapiro steps. Then, Ch. 3 investigates the influence of thermal, resistive noise on the dual Shapiro step

height. Here, we discuss how the Bloch oscillation frequency and the dual Shapiro steps are being washed out by thermal fluctuations. Additionally, we provide an analytical result for the minimum step height needed in order to observe the steps in presence of thermal fluctuations.

After studying all these properties in an ideal circuit, we add the parasitic capacitance as well as the superinductance to our system. In Ch. 4, we describe the resulting system by a Schrödinger equation which is coupled to a classical equation of motion. Furthermore, we discuss the influence of a small capacitance parallel to the superinductance which can not be avoided in experimental setups. Building on this characterization of the system, Ch. 5 focuses on the calculation of the dual Shapiro step height in the extended circuit. We start by investigating the ideal regime of high impedance where the characteristic impedance, $Z = \sqrt{L/C_p}$, formed by the superinductance L and the parasitic capacitance C_p, is larger than the quantum resistance $R_Q = h/4e^2 \approx 6.5\,\mathrm{k\Omega}$. Next, we examine the experimentally more relevant regime $Z \simeq R_Q$, where quantum effects play an important role. Finally, we validate our analytical results by comparing them to numerical simulations.

1.2 Duality of Josephson and Bloch oscillations

A quantum phase-slip junction is the exact dual counterpart to the Josephson junction. This means that, compared to an ordinary Josephson junction, the role of the phase ϕ across the junction and the charge Q on the capacitor plates is interchanged. Additionally, the process of Cooper-pair tunneling is replaced by its dual counterpart, a 2π slippage of the phase-difference between the two superconductors composing the Josephson junction [7].

The equations governing the behavior of the phase-slip junction are, therefore, exactly dual to the usual Josephson relations. For a regular Josephson junction, the current, $I_J = I_c \sin(\phi)$, is a periodic function of the phase, where I_c is the critical current of the junction. The voltage across the Josephson junction is given by the time derivative of the phase $V_J = (\hbar/2e)d\phi/dt$. Dual to this, the voltage of the phase-slip junction $V_P = V_c \sin(\pi Q/e)$ is a periodic function of the charge and the current $I_P = dQ/dt$ is only different from zero for time dependent charge.

Due to these relations, the phase-slip junction exhibits behaviors dual to the

DC- and AC-Josephson effect. The DC-Josephson effect refers to a Josephson junction maintaining a current without any applied voltage. A phase-slip junction can, in turn, sustain a voltage without any applied current. The AC-Josephson effect occurs when a constant voltage is applied to a regular Josephson junction. This leads to an oscillating current, so-called Josephson oscillations — the exact dual counterpart to the previously introduced Bloch oscillations. If the Josephson junction is additionally irradiated with microwaves of frequency ω_0, phase-locking between the Josephson oscillations and the external microwaves causes conventional Shapiro steps of constant voltage to appear at multiples of $\hbar\omega_0/2e$.

However, due to the fundamental asymmetry between electric and magnetic effects in matter, the dual and the conventional Shapiro steps are physically quite different. In particular, the dual equivalent to the parasitic capacitance – an inductance of the leads [8] – is, unlike its counterpart, easily reduced in experimental setups. Thus, Shapiro steps have already been observed in multiple systems since their first discovery in the 60s [9]. As the step position is related only to fundamental constants of physics, Shapiro steps can be used in metrology to define the quantum voltage standard [10].

Chapter 2

Dual Shapiro steps in an ideal setup

2.1 Josephson junction in the phase-slip regime

In order to understand dual Shapiro steps, we first need to understand the concept of phase-slip junctions. A phase-slip junction can be implemented by a small Josephson junction with a Josephson energy $E_J = \Phi_0 I_c/2\pi$ and a finite capacitance C, where $\Phi_0 = h/2e$ denotes the superconducting flux quantum and I_c the critical current of the junction. Figure 2.1(a) shows the circuit of such a Josephson junction connected to an external current source. The Lagrangian of this system is given by

$$\mathcal{L} = \frac{C}{2}\dot{\phi}^2 + E_J\left[\cos\left(\frac{2\pi\phi}{\Phi_0}\right) - 1\right] - Q\dot{\phi}, \tag{2.1}$$

assuming that there is no external magnetic flux [8]. Here, the first two terms are due to the Josephson junction and its associated capacitance. They are described in terms of the node flux ϕ, where the derivative of the flux $\dot{\phi}$ represents the voltage across the junction. Multiplying this voltage with the charge Q transported onto the capacitor plates by the current source yields the last term of the Lagrangian, guaranteeing Kirchhoff's voltage and current law. Introducing the charge $q = \partial\mathcal{L}/\partial\dot{\phi}$, the canonically conjugate variable to ϕ, we can perform the Legendre transformation and obtain the Hamiltonian

$$\hat{H} = \frac{(\hat{q}+Q)^2}{2C} + E_J\left[1 - \cos\left(\frac{2\pi\hat{\phi}}{\Phi_0}\right)\right], \tag{2.2}$$

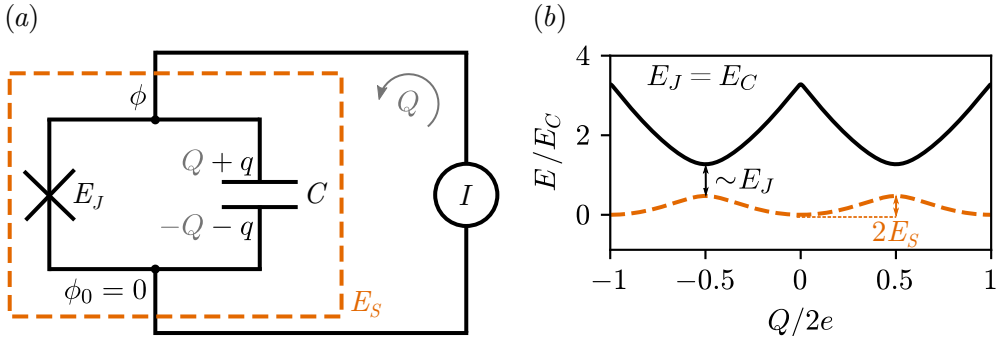

Figure 2.1: (a) Small Josephson junction with Josephson energy E_J and finite capacitance C connected to an external current source. The current source provides the current $I = \dot{Q}$. Under the appropriate conditions, the Josephson junction acts as a phase-slip junction with phase-slip energy E_S. (b) Energy spectrum of the illustrated system for $E_J = E_C$. The band gap between the ground state and the first excited state scales with E_J. The band structure is $2e$-periodic in Q. The phase-slip energy E_S corresponds to the bandwidth of the lowest energy band.

where the operators obey the commutator relation $[\hat{q}, \hat{\phi}] = i\hbar$. The eigenvalue spectrum of the Hamiltonian is $2e$-periodic in Q and shown in Fig. 2.1(b) for $E_J = E_C = e^2/2C$.

For a charging energy E_C much larger than the Josephson energy E_J, the influence of the periodic potential due to the Josephson junction is negligible. Here, the energy bands correspond to the bands of the nearly free electron approximation in solid state physics. Since the band gaps are very small, even a small external current can cause Landau-Zener tunneling to higher bands [11].

A small charging energy, $E_C \ll E_J$, corresponds to a particle of high mass which always remains close to the minimum of the potential. In this limit, we can, thus, neglect the periodicity of the Josephson potential and instead approximate the cosine by a harmonic potential. This results in flat bands spaced apart equally by the energy scale of the harmonic oscillator $\sqrt{8E_C E_J}$, see also App. A.

However, we are most interested in the regime $E_C \lesssim E_J$. Here, the first and second band are already well separated but the energy of the lowest band still depends strongly on Q. First order perturbation theory for small E_J/E_C finds that the band gap scales with E_J [12]. Dependent on the external current I,

this results in the Landau-Zener transition probability

$$P_{\mathrm{LZ}} = \exp\left(-\frac{\pi}{16}\frac{E_J}{E_C}\frac{E_J}{\hbar I/2e}\right) \tag{2.3}$$

between the first and second band [12]. If the system is to remain in the lowest band, the current has to be restricted to $I \ll E_J^2/E_C\Phi_0$. Under this condition, the Landau-Zener transition probability is small and we can describe the Josephson junction using only the lowest band of the energy spectrum. A Josephson junction operated in this regime is called a phase-slip junction.

For $E_C \lesssim E_J$, the ground state energy can be approximated by a single cosine function, $E_P = -E_S\cos(\pi Q/e)$, where the phase-slip energy E_S corresponds to the bandwidth of the lowest band. Equivalently, the voltage across the junction is given by $V_P = dE_P/dQ = V_c\sin(\pi Q/e)$, with $V_c = \pi E_S/e$ the critical voltage of the phase-slip junction. In App. A, we calculate the phase-slip energy using the semi-classical WKB-method. There, we obtain

$$E_S \simeq E_C^{1/4}E_J^{3/4}e^{-\sqrt{8E_J/E_C}}. \tag{2.4}$$

We come back to this relation, when we discuss the influence of the parasitic capacitance in Sec. 4.1.

For the remainder of this thesis, we always assume that the external current is small enough such that the Josephson junction can be approximated by a phase-slip junction. Additionally, we describe the voltage-charge relation of the phase-slip junction only by a single sine function $V_P = V_c\sin(\pi Q/e)$ neglecting contributions of higher frequencies. For the following calculations, it is also useful to introduce the capacitance $C_S = e/\pi V_c$ associated with the phase-slip junction.

2.2 Emergence of Bloch oscillations

In this section, we consider a phase-slip junction, with critical voltage V_c, in series with a voltage source, supplying the voltage V, and a resistance R. The corresponding ideal circuit is shown in Fig. 2.2. The voltage source, together with the resistance R, forms a current source providing the current I. The step to a quantum description of the problem is performed by introducing the loop charge operator $\hat{Q} = \int_{-\infty}^{t} dt'\hat{I}(t')$ which denotes the charge that has flown in the loop up to a time t [8]. Using Kirchhoff's voltage law, we can derive an

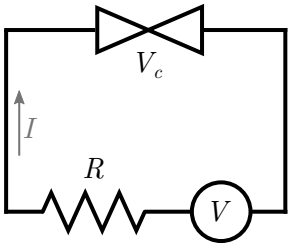

Figure 2.2: Ideal setup for the observation of dual Shapiro steps. The circuit consists of a phase-slip junction, with critical voltage V_c, in series with a resistance R and an ideal voltage source, supplying the voltage V. The voltage source, together with the large resistance R, acts as a current source providing the current I.

equation of motion for the loop charge

$$R\dot{\hat{Q}} + V_c \sin\left(\frac{\pi}{e}\hat{Q}\right) = V(t). \tag{2.5}$$

Here, we include only the noiseless, classical part of the voltage source as we assume that the system is operated at low temperature. The condition under which this assumption is justified is discussed in Ch. 3, where we study the influence of thermal noise on the system.

While the quantum mechanical description becomes important in Ch. 4, in this chapter, we focus on the purely classical regime. For the ideal circuit, this regime is easily realized by a large resistances R with $R \gg R_Q$. In this limit, the quantum fluctuations of $\hat{Q}$ are suppressed far below $2e$ [13], such that the operator can be simply replaced by its quantum-mechanical expectation value $Q = \langle\hat{Q}\rangle$.

In this section, we consider the case where the voltage source supplies only a DC-voltage, $V(t) = V_{0,\mathrm{dc}}$. First, we examine the case $V_{0,\mathrm{dc}} < V_c$. Here, the drive is too small for the charges to overcome the potential barrier of the phase-slip junction. Thus, after an initial transient response, no current flows through the junction. This so-called Coulomb blockade [14] causes a voltage step at zero current in the IV-curve, as shown in Fig. 2.3.

Next, we study the more interesting case $V_{0,\mathrm{dc}} > V_c$, where the drive is strong enough to generate a current $I_{\mathrm{dc}} = \dot{Q}_{\mathrm{dc}}$. In order to simplify the following calculations, we divide Eq. (2.5) by V_c and introduce the normalized charge $N_{\mathrm{dc}} = \pi Q_{\mathrm{dc}}/e$. We obtain

$$\frac{\dot{N}_{\mathrm{dc}}}{\omega_R} + \sin(N_{\mathrm{dc}}) = v_{0,\mathrm{dc}}, \tag{2.6}$$

where $v_{0,\mathrm{dc}} = V_{0,\mathrm{dc}}/V_c$ is the normalized DC-drive and $\omega_R = \pi V_c/eR = 1/RC_S$ the RC-rate with which the motion of the charge is damped. This differential

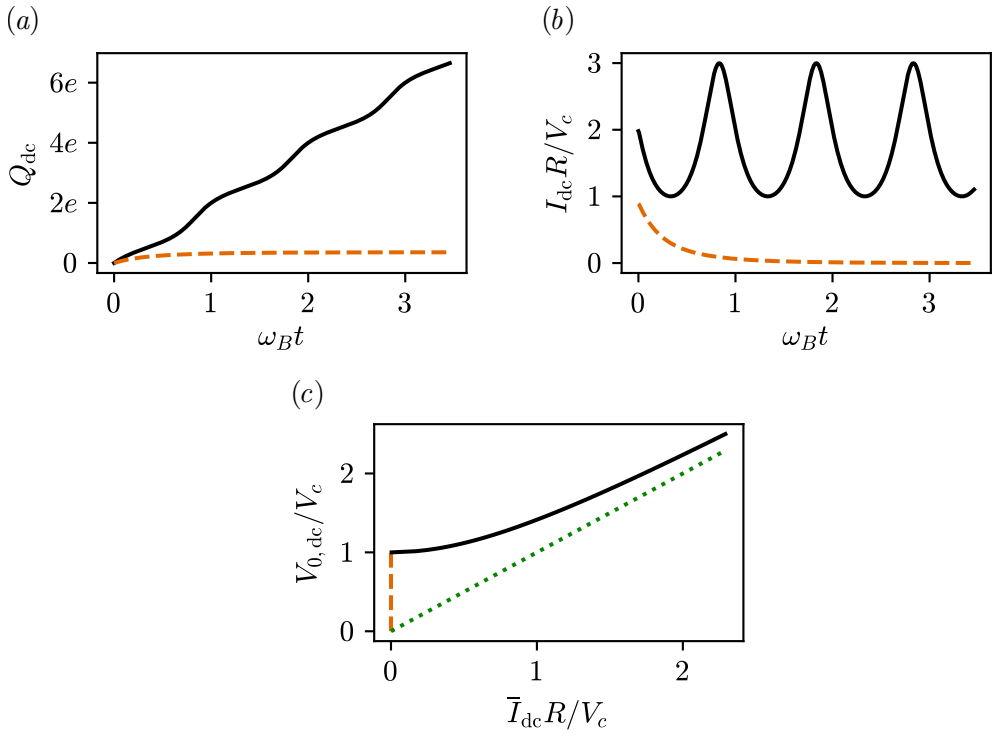

Figure 2.3: (*a*), (*b*) Time-evolution of the charge Q_{dc} and the current I_{dc} in presence of a DC-drive. The orange, dashed line displays the result for $V_{0,\mathrm{dc}} = 0.9V_c$. The black, solid line shows the result for $V_{0,\mathrm{dc}} = 2V_c$. For $V_{0,\mathrm{dc}} < V_c$, the charge approaches a constant value below $e/2$ and no current flows through the junction. For $V_{0,\mathrm{dc}} > V_c$, the current oscillates around its average value $\overline{I}_{\mathrm{dc}}$ with the Bloch oscillation frequency ω_B. (*c*) Subsequent IV-curve of a DC-biased phase-slip junction. The Coulomb blockade step at $\overline{I}_{\mathrm{dc}} = 0$ is clearly visible. For $V_{0,\mathrm{dc}} \gg V_c$, the average current approaches an ohmic dependence on the DC-drive, as indicated by the green, dotted line.

equation is separable and can be solved with the result[1] [15]

$$N_{\mathrm{dc}}(t) = 2\arctan\left\{\frac{i_0}{v_{0,\mathrm{dc}}-1}\tan\left[\frac{\omega_B\,(t-t_0)+\pi/2}{2}\right]\right\} - \frac{\pi}{2}, \tag{2.7}$$

$$I_{\mathrm{dc}}(t) = \frac{i_0^2}{v_{0,\mathrm{dc}} + \sin[\omega_B\,(t-t_0)]}\frac{V_c}{R}. \tag{2.8}$$

Here, $i_0 = \overline{I}_{\mathrm{dc}}R/V_c = (v_{0,\mathrm{dc}}^2 - 1)^{1/2}$ is the normalized, average current and $\omega_B = \omega_R\, i_0 = \pi\overline{I}_{\mathrm{dc}}/e$ the Bloch oscillation frequency. The initial condition can always be fulfilled by choosing an appropriate time-shift t_0. The current I_{dc}

[1] Note that the solution for N_{dc} needs to be analytically continued to obtain a physical solution over more than one period.

can be decomposed into its Fourier components

$$I_{\mathrm{dc}}(t) = \sum_{k=-\infty}^{\infty} I_k e^{ik\omega_B(t-t_0)}, \qquad I_k = i^k \frac{i_0}{(i_0 + v_{0,\mathrm{dc}})^{|k|}} \frac{V_c}{R}. \tag{2.9}$$

Figure 2.3 displays the time-evolution of charge and current as well as the subsequent IV-curve. We can clearly see that the DC-drive causes the current to oscillate around its average value with the Bloch oscillation frequency ω_B. For large enough drive $v_{0,\mathrm{dc}} \gg 1$ the average current approaches an ohmic dependence on the DC-voltage $\overline{I}_{\mathrm{dc}} = V_{0,\mathrm{dc}}/R$.

2.3 Phase-locking with an AC-drive

After considering the case of a pure DC-drive in the last section, we now combine the DC-drive with an additional AC-component, $V(t) = V_0 + V_{\mathrm{ac}} \sin(\omega_0 t)$. The microwaves can phase-lock with the Bloch oscillations caused by the DC-bias. This leads to voltage steps at constant current in the IV-curve, so-called dual Shapiro steps. For the system described by Eq. (2.5), phase-locking is only possible if the Bloch frequency ω_B is an integer multiple of the drive frequency ω_0. Consequently, the steps appear at multiples of $I_S = e\omega_0/\pi$ ($i_S = I_S R/V_c = \omega_0/\omega_R$).

We want to calculate the height of the dual Shapiro steps. Analogously to the previous section, we consider the equation of motion

$$\frac{\dot{N}}{\omega_R} + \sin(N) = v_0 + v_{\mathrm{ac}} \sin(\omega_0 t), \tag{2.10}$$

with $v_{\mathrm{ac}} = V_{\mathrm{ac}}/V_c$. In the following, we assume that the amplitude of the AC-drive is much smaller than the critical voltage $v_{\mathrm{ac}} \ll 1$. In this case, we can expand the solution to Eq. (2.10) in a Taylor series $N = N_{\mathrm{dc}} + v_{\mathrm{ac}} N_{\mathrm{ac}}$. Additionally, we need to take into account that phase-locking between the Bloch oscillations and the AC-drive can change the average voltage. Therefore, we formally expand the DC-drive $v_0 = v_{0,\mathrm{dc}} + v_{\mathrm{ac}}\, v_{0,\mathrm{ac}}$ in a Taylor series, too. Here, $v_{0,\mathrm{ac}}$ corresponds to the change of the DC-voltage on the step due to the AC-drive. In order to estimate the dual Shapiro step height, we, thus, have to calculate $v_{0,\mathrm{ac}}$.

Substituting both expansions into Eq. (2.10) yields the system of equations [15]

$$\frac{\dot{N}_{\mathrm{dc}}}{\omega_R} + \sin(N_{\mathrm{dc}}) = v_{0,\mathrm{dc}}, \tag{2.11}$$

$$\frac{\dot{N}_{\mathrm{ac}}}{\omega_R} + \cos(N_{\mathrm{dc}})N_{\mathrm{ac}} = v_{0,\mathrm{ac}} + \sin(\omega_0 t). \tag{2.12}$$

The first equation is identical to Eq. (2.6) and has already been solved for $v_{0,\mathrm{dc}} > 1$ in the previous section. The second equation is a differential equation for N_{ac}. However, this equation does not need to be solved in order to obtain the dual Shapiro step height. Instead, we have to take into account that the average current on the step remains constant. Therefore, we have to require that the AC-drive does not add a DC-component to the current, $\overline{\dot{N}}_{\mathrm{ac}} = 0$. We make the substitution

$$N_{\mathrm{ac}} = N'_{\mathrm{ac}} e^{-\omega_R \int_{-\infty}^{t} \cos[N_{\mathrm{dc}}(t')]dt'} = N'_{\mathrm{ac}} \dot{N}_{\mathrm{dc}}, \tag{2.13}$$

where the last step can be obtained by differentiating Eq. (2.11) with respect to time. Since $\dot{N}_{\mathrm{dc}}$ is a periodic function, the constraint $\overline{\dot{N}}_{\mathrm{ac}} = 0$ directly translates to the same constraint for N'_{ac}. Inserting Eq. (2.13) into Eq. (2.12), we obtain the condition

$$\overline{\left[v_{0,\mathrm{ac}} + \sin(\omega_0 t)\right] / \dot{N}_{\mathrm{dc}}} = 0, \tag{2.14}$$

which only depends on the DC-solution. To obtain the height of the first dual Shapiro step, we set the Bloch oscillation frequency ω_B equal to the drive frequency ω_0 and calculate the time average. We receive an equation for $v_{0,\mathrm{ac}}$

$$v_{0,\mathrm{ac}} = -\frac{\cos(\omega_0 t_0)}{2v_{0,\mathrm{dc}}}. \tag{2.15}$$

Dependent on the position on the voltage step, $v_{0,\mathrm{ac}}$ and, thus, the phase shift t_0 between the Bloch oscillations and the AC-drive varies. This means that, for all voltages on the step, the system compensates the changing DC-bias by adjusting the phase shift between the oscillations.

Figure 2.4 shows a typical IV-curve of a phase-slip junction under microwave irradiation. At the bottom of the first step, the Bloch oscillations and the drive are completely out-of-phase. In our calculation, this corresponds the case $t_0 = 0$ with $V_0 = V_{0,\mathrm{dc}} - V_{\mathrm{ac}}/2v_{0,\mathrm{dc}}$. For $t_0 = \pi/\omega_0$, both oscillations are perfectly in-phase which corresponds to the top of the step at $V_0 = V_{0,\mathrm{dc}} + V_{\mathrm{ac}}/2v_{0,\mathrm{dc}}$. The

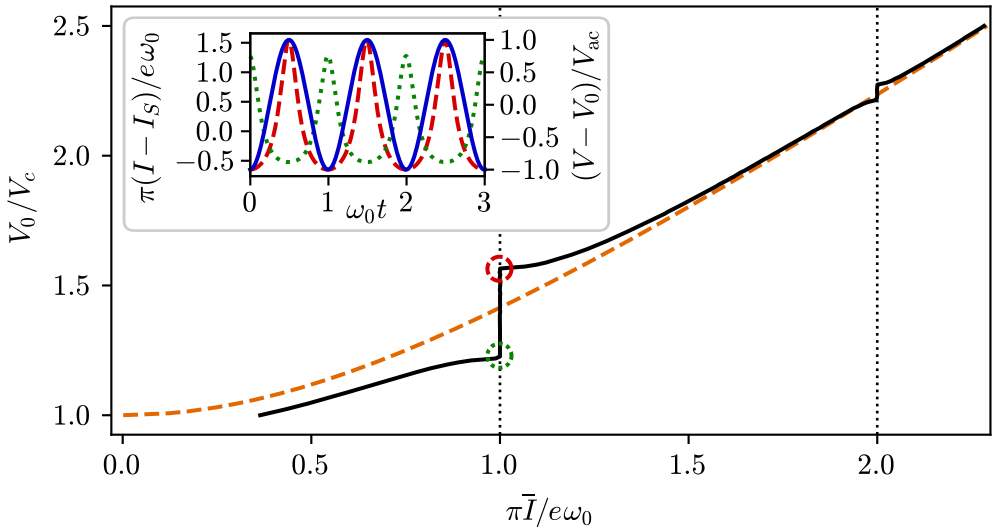

Figure 2.4: IV-curve of a DC-biased phase-slip junction under microwave irradiation with $V_{ac} = 0.5V_c$ and $\omega_0 = \omega_R$ (black, solid). For comparison, the IV-curve of a solely DC-biased phase-slip junction is included as an orange, dashed line. Dual Shapiro steps develop symmetrically around the DC-biased curve at multiples of $I_S = e\omega_0/\pi$. At the first step the drive frequency ω_0 and the Bloch frequency ω_B are identical. The inlay displays the phase shift between the AC-drive (blue, solid) and the current at the bottom (green, dotted) and at the top (red, dashed) of the first step. At the bottom of the step, the drive and the current are out-of-phase. At the top of the step, both oscillations are in-phase.

total dual Shapiro step height is, thus, given by

$$\Delta V = \frac{V_{ac}}{\sqrt{1 + (\omega_0/\omega_R)^2}}, \tag{2.16}$$

valid to first order in V_{ac}/V_c. Here, we used the relation $v_{0,dc} = (i_S^2 + 1)^{1/2}$ which we derived in the previous section. From this it also follows that the voltage around which the step is centered can be written as

$$V_S = V_c\sqrt{1 + (\omega_0/\omega_R)^2}. \tag{2.17}$$

If we wanted to calculate the height of the second or third dual Shapiro step, we would have to include higher orders of V_{ac}/V_c. However, since the first step is the largest and, therefore, the easiest to measure, we are going to focus on this step for the remainder of this thesis.

In order to check our results, we have calculated the step height and step position numerically by solving Eq. (2.10). The results can be found in Fig. 2.5

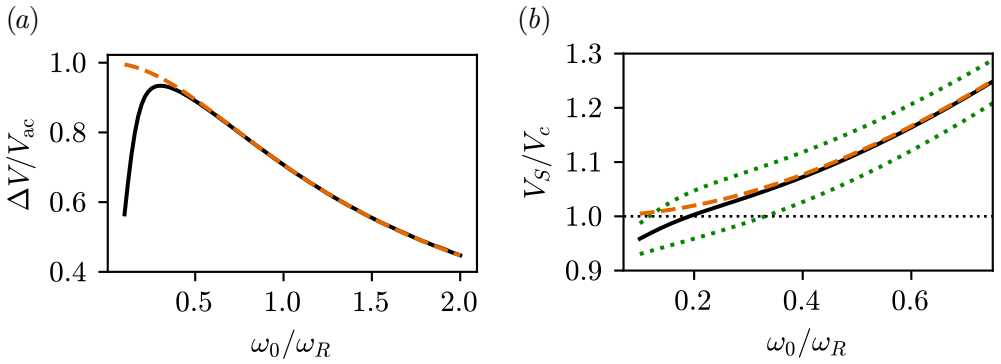

Figure 2.5: (*a*) Dual Shapiro step height as a function of the drive frequency ω_0 for $V_{\mathrm{ac}} = 0.1V_c$. The black, solid line displays the numerical solution of Eq. (2.10). The orange, dashed line shows the analytical result of Eq. (2.16). The analytical result fits the numerical data well, except for small ω_0/ω_R where the numerical step height is smaller than the predicted height. (*b*) Dual Shapiro step position as a function of the drive frequency ω_0 for $V_{\mathrm{ac}} = 0.1V_c$. The black, solid line displays the numerical result while the orange, dashed line shows the analytical result in Eq. (2.17). The green, dotted lines indicate the positions of the lower and upper corners of the Shapiro step. As long as the entire step appears at voltages above the critical voltage V_c, the analytical result fits the numerical data well. Below that point, higher order effects decrease the numerically calculated step height.

together with the analytical results. We find that the analytical results fits the numerical data well as long as the entire step appears at voltages above the critical voltage V_c. Due to the additional AC-drive, it is possible to obtain average currents different from zero even for DC-biases V_0 smaller than the critical voltage V_c, as predicted by the analytical results. However, in this regime, there are no initial Bloch oscillations caused by the DC-bias which can simply phase-lock with the AC-drive as we assumed throughout our calculations. Instead, the AC-drive is needed to overcome the Coulomb blockade and cause Bloch oscillations. These higher order effects cause the step height to decline. Thus, Eq. (2.16) is no longer valid in this limit and the maximum step height V_{ac} is never reached.

In addition, we used numerical simulations to show how the step height depends on the amplitude of the AC-drive V_{ac}. An exemplary result for a drive frequency $\omega_0 = 2\omega_R$ can be found in Fig. 2.6. In the regime $V_{\mathrm{ac}} \ll V_c$, the step height increases linearly with the amplitude as predicted by the first order approximation. For $V_{\mathrm{ac}} \gtrsim V_c$, the AC-drive is no longer a small perturbation that phase-locks with the nearly undisturbed Bloch oscillations caused by a much larger DC-bias. Instead, the AC-drive itself is large enough to overcome the potential barrier set by the phase-slip junction and can, thus, cause a current

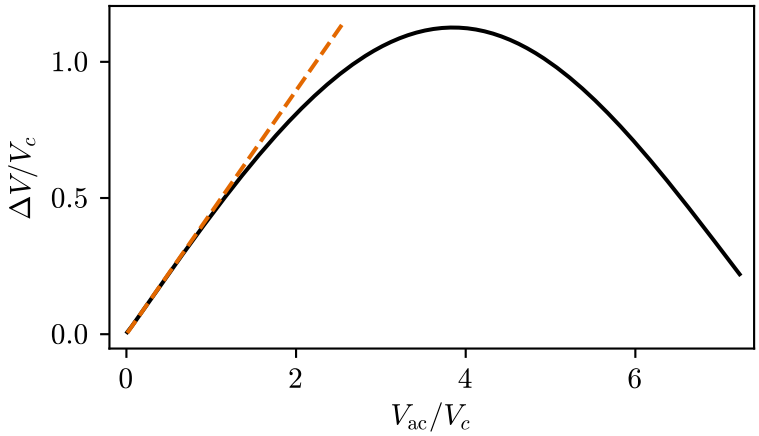

Figure 2.6: Dual Shapiro step height as a function of the AC-drive amplitude V_{ac} for $\omega_0 = 2\omega_R$. The black, solid line displays the numerical solution of Eq. (2.10). The orange, dashed line shows the first order approximation in Eq. (2.16). The analytical result corresponds very well to the numerical data for $V_{\mathrm{ac}} \ll V_c$. A maximum step height is reached for $V_{\mathrm{ac}} \approx 4V_c$, where the step height starts to decrease again.

to flow through the junction. This, in turn, influences the Bloch oscillation frequency leads to a maximum step height at $V_{\mathrm{ac}} \approx 4V_c$. For higher amplitudes the dual Shapiro step height starts to decrease again.

Next, we want to investigate the behavior of the system close to the dual Shapiro step. As evidenced by Fig. 2.4, the first dual Shapiro step resembles qualitatively the shape of the Coulomb blockade step at $I_0 = 0$. The reason for this resemblance is as follows.

Instead of setting the Bloch oscillation frequency exactly equal to the drive frequency as before, we now consider frequencies $\omega_B \neq \omega_0$ ($i_0 \neq i_S$). Away from the step, the phase shift t_0 is no longer important and we neglect it in the following calculations. However, we are still interested in the behavior of the junction close to the first step. When performing the time averaging in Eq. (2.14), we, therefore, average over time scales Δt with $\omega_0^{-1}, \omega_B^{-1} \ll \Delta t \ll |\omega_0 - \omega_B|^{-1}$. We obtain

$$v_{0,\mathrm{ac}} = -\frac{\cos[(\omega_0 - \omega_B)t]}{2v_{0,\mathrm{dc}}} = -\frac{\cos[\pi(Q_S - Q_0)/e]}{2v_{0,\mathrm{dc}}}. \tag{2.18}$$

In the last step, we have introduced the average, cumulative charges $Q_S = I_S t$ and $Q_0 = I_0 t$. Here, Q_S corresponds to the charge flowing through the system at the step, while Q_0 corresponds to a general average charge away from the step position I_S. Next, we expand the relation $I_0 = \dot{Q}_0 = V_c[(v_0 - v_{\mathrm{ac}} v_{0,\mathrm{ac}})^2 - 1]^{1/2}/R$

to first order in $v_{0,\mathrm{ac}}$ and insert Eq. (2.18). We obtain

$$\dot{Q}_0 = \underbrace{\frac{V_c}{R}\sqrt{v_0^2-1}}_{I_0} + \overbrace{\frac{v_0}{R\sqrt{v_0^2-1}}}^{R_d^{-1}} \underbrace{\frac{V_{\mathrm{ac}}}{2v_{0,\mathrm{dc}}}}_{\Delta V/2} \cos\left[\frac{\pi}{e}(Q_S - Q_0)\right], \tag{2.19}$$

where $R_d = dV_0/dI_0$ is the differential resistance at the step in absence of an AC-drive[2] [15]. Next, we rewrite Eq. (2.19) to obtain a differential equation for[3] $\delta Q = Q_0 - Q_S + e/2$

$$R_d\,\delta\dot{Q} + \frac{\Delta V}{2}\sin\left(\frac{\pi}{e}\delta Q\right) = \tilde{V}_0 - \tilde{V}_S, \tag{2.20}$$

with $\tilde{V}_{0[S]} = R_d I_{0[S]}$. This result coincides with Eq. (2.5), for an imaginary DC-biased phase-slip junction with critical voltage $\Delta V/2$ and normal resistance R_d. Here, the relevant DC-voltage is the difference between the voltage at the center of the step $\tilde{V}_S$ and the applied voltage $\tilde{V}_0$. We, thus, find that the behavior of the system close to the first dual Shapiro step can be mapped onto a phase-slip junction at the Coulomb blockade. This property becomes useful when we explore the influence of thermal noise on the step height in the next chapter.

We comment on the experimental parameters of the discussed setup. Nowadays, it is possible to fabricate Josephson junctions with E_J/h, $E_C/h \simeq 10\,\mathrm{GHz}$ [16], which results in critical voltages V_c of the order of $10\,\mu\mathrm{V}$ ($C_S \simeq 5\,\mathrm{fF}$). In order to avoid Landau-Zener processes, the drive frequency $\omega_0/2\pi$ should, thus, remain well below 10 GHz. Therefore, the dual Shapiro steps appear at currents of the order of nano-amps. In this context, note that a current standard formed by Shapiro steps is readily parallelizable in order to achieve larger values [2].

[2]Note that here I_0 and R_d take into account the full DC-current V_0 instead of $V_{0,\mathrm{dc}}$

[3]Note that the term $e/2$ is only added in order to reproduce the sine function in Eq. (2.5). It has no physical significance.

Chapter 3

Influence of thermal fluctuations

3.1 Introduction to noise

In the previous chapter, we have discussed the emergence of Bloch oscillations and dual Shapiro steps at zero temperature. Here, we treat the case of finite temperature and investigate the influence of thermal noise on the dual Shapiro step height. We start by discussing some general properties of noise and the Johnson-Nyquist formula.

A general noise signal $\xi(t)$ with $\langle \xi(t) \rangle = 0$ can be characterized by the auto-correlation

$$\langle \langle \xi(t)\xi(0) \rangle \rangle = \langle \xi(t)\xi(0) \rangle = f(t), \tag{3.1}$$

where $\langle \cdot \rangle$ denotes the ensemble average. The spectral density of the noise $S(\omega)$ is given by the Fourier transform of the auto-correlation

$$S(\omega) = \int_{-\infty}^{\infty} dt\, e^{i\omega t} f(t), \qquad f(t) = \frac{1}{2\pi} \int_{-\infty}^{\infty} d\omega\, e^{-i\omega t} S(\omega). \tag{3.2}$$

Since the auto-correlation is an even, real function, the spectral density is even and real, too. Additionally, the spectral density can be expressed in terms of the correlation of the noise signal in Fourier space

$$2\pi S(\omega)\delta(\omega + \omega') = \langle \langle \xi^*(\omega')\xi(\omega) \rangle \rangle. \tag{3.3}$$

In this and the following section, we focus on thermal, white noise. Colored noise is treated in Sec. 3.3. White noise has a constant spectral density $S(\omega) \equiv S(0)$ and, thus, the correlation is given by $f(t) = S(0)\,\delta(t)$. The strength of the

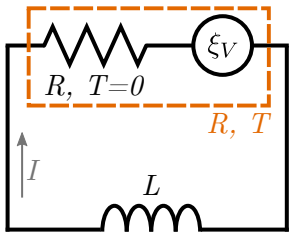

Figure 3.1: Circuit representation of a resistor at finite temperature shunted by an inductance. A resistor with resistance R at finite temperature T can be represented by a resistor at zero temperature in series to a voltage noise source $\xi_V(t)$. The resistor is shunted by an inductance L. The current flowing through the resistor is denoted by I.

fluctuations is determined by the Johnson-Nyquist formula [17,18]. In order to derive this formula, we have to take a closer look at a resistor at finite temperature.

The thermal motion of electrons in a resistor gives rise to fluctuating resistance values and, therefore, produces a fluctuating voltage across the resistor. It can be shown that a resistor at finite temperature T can be represented by an 'ideal' resistor R at zero temperature in series to a voltage noise source $\xi_V(t)$ [18]. Additionally, the spectral density of this voltage noise does not depend on the individual impedance connected to the resistor [18]. For the purpose of the following derivation, we can, thus, choose to shunt the resistor by an inductance L [19], as shown in Fig. 3.1. The equation of motion for the fluctuating current I in the loop is given by

$$L\dot{I} + RI = \xi_V(t). \tag{3.4}$$

This first order differential equation can be solved for a general $\xi_V(t)$ to obtain

$$I(t) = \frac{1}{L}\int_{-\infty}^{t} dt' e^{-R(t-t')/L}\,\xi_V(t'). \tag{3.5}$$

The average current is zero and the calculation of the variance of the current $\langle\langle I(t)^2\rangle\rangle = \langle I(t)^2\rangle$ is straightforward

$$\begin{aligned}\langle\langle I(t)^2\rangle\rangle &= \frac{1}{L^2}\int_{-\infty}^{t} dt' \int_{-\infty}^{t} dt'' e^{-R(2t-t'-t'')/L} \underbrace{\langle\langle \xi_V(t')\xi_V(t'')\rangle\rangle}_{S_V(0)\,\delta(t'-t'')} \\ &= \frac{S_V(0)}{L^2}\int_{-\infty}^{t} dt' e^{-R(2t-2t')/L} = \frac{S_V(0)}{2RL}.\end{aligned} \tag{3.6}$$

Additionally, the potential energy stored in the magnetic field of the inductance, $LI^2/2$, determines the kinetic energy of the thermal motion of the charges and vice versa. Due to the equipartition theorem, we know that $\langle LI^2/2\rangle = k_B T/2$, with k_B is the Boltzmann constant. By comparing the result of the equipartition

theorem to Eq. (3.6), we obtain the spectral density

$$S_V(0) = 2Rk_BT. \tag{3.7}$$

This solution is widely known as the Johnson-Nyquist formula[1] and demonstrates the fluctuation-dissipation theorem. The resistor dissipates electrical energy, turning it into heat, which in turn causes the fluctuations.

3.2 Impact of noise on the dual Shapiro step height

In this section, we discuss the influence of thermal, white noise on the height of the dual Shapiro step. Analogously to Ch. 2, we consider the ideal circuit of a phase-slip junction in series with a resistor and a voltage source, described by Eq. (2.6) and depicted in Fig. 2.2.

To begin with, we calculate how resistive noise washes out the Coulomb blockade step centered around zero voltage. Thus, we set $v_{0,\mathrm{dc}} = 0$ and only consider the influence of the fluctuations $\xi_V(t)$. For sufficiently small noise, we can additionally linearize the sine-function in Eq. (2.6) and obtain

$$\frac{\dot{N}_f}{\omega_R} + N_f = \frac{\xi_V(t)}{V_c}. \tag{3.8}$$

This differential equation is of the same form as Eq. (3.4). For thermal, white noise, we can, thus, take steps equivalent to Eqs. (3.5) and (3.6) to calculate the variance of the normalized charge fluctuations with the result

$$\langle\langle N_f^2\rangle\rangle = \frac{k_BT}{E_S} = \gamma_0, \tag{3.9}$$

where we used the Johnson-Nyquist formula in Eq. (3.7). This result can be interpreted as follows. For $\gamma_0 \ll 1$, the deviations of the charge are small and the average charge is still subject to the periodic potential of the phase-slip junction. Here, the thermal energy is not large enough to overcome the potential barrier set by the phase-slip energy. The Coulomb blockade step is clearly visible. For $\gamma_0 \gtrsim 1$, the thermal energy is larger than the phase-slip energy. Therefore, the deviations are of the scale or larger than the periodicity of the potential. The Coulomb blockade step is washed out. Figure 3.2 displays the

[1] Note that the spectral density for the Johnson-Nyquist noise is often taken as $S_V(0) = 4Rk_BT$. Here, we defined the spectral density for both positive and negative frequencies, while other authors define the spectral density only for physical (positive) frequencies. This causes the additional factor of 2.

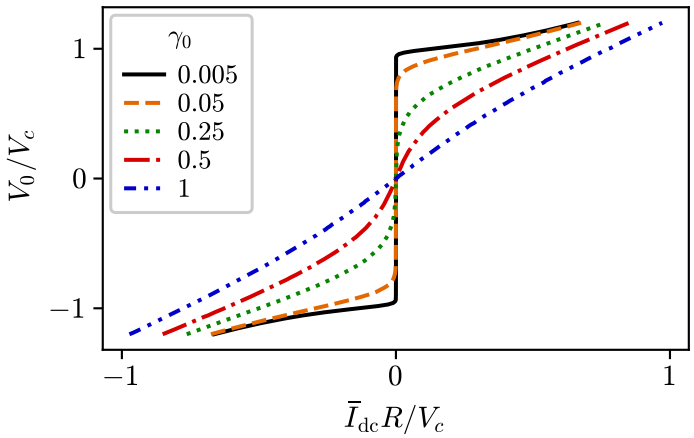

Figure 3.2: Coulomb blockade step at zero current under the influence of thermal, white noise. The results were obtained by solving Eq. (2.6) numerically and including thermal fluctuations with different values of the effective noise parameter γ_0. For $\gamma_0 = 1$, the step is completely washed out by thermal fluctuations.

Coulomb blockade step for different values of the effective noise parameter γ_0. As predicted, the step is completely washed out for $\gamma_0 \simeq 1$, where the fluctuations are of the same scale as the periodicity of the potential.

Next, we investigate the influence of noise on the first dual Shapiro step. Analogously to Eq. (3.8), we can rewrite Eq. (2.20) as

$$\frac{eR_d}{\pi}\delta\dot{N} + \frac{\Delta V}{2}\delta N = \xi_V'(t), \tag{3.10}$$

with $\xi_V'(t)$ the effective noise around the first step with frequency components close to the Bloch frequency. This noise term is obtained by averaging Eq. (2.14) with the original noise term $\xi_V(t)$

$$\xi_V'(t) = \overline{\xi_V(t)\sin(\omega_B t)}/v_{0,\mathrm{dc}}, \tag{3.11}$$

where the averaging is over time scales Δt with $\omega_0^{-1}, \omega_B^{-1} \ll \Delta t \ll |\omega_0 - \omega_B|^{-1}, \Gamma_1^{-1}$. Note that here we have introduced the linewidth Γ_1 of the current spectral density around the Bloch frequency ω_B, as displayed in Fig. 3.3. Before we continue with the calculation of the effective noise parameter γ_1 for the first dual Shapiro step, we want to explain the origin of this linewidth.

The fluctuations $\xi_V(t)$ with spectral density $S_V(0)$ induce current fluctuations $\xi_I(t)$ with some frequency spectrum $S_I(\omega)$. Since the Bloch oscillation frequency $\omega_B = \pi I_0/e$ depends on the average current, it is forced to fluctuate around

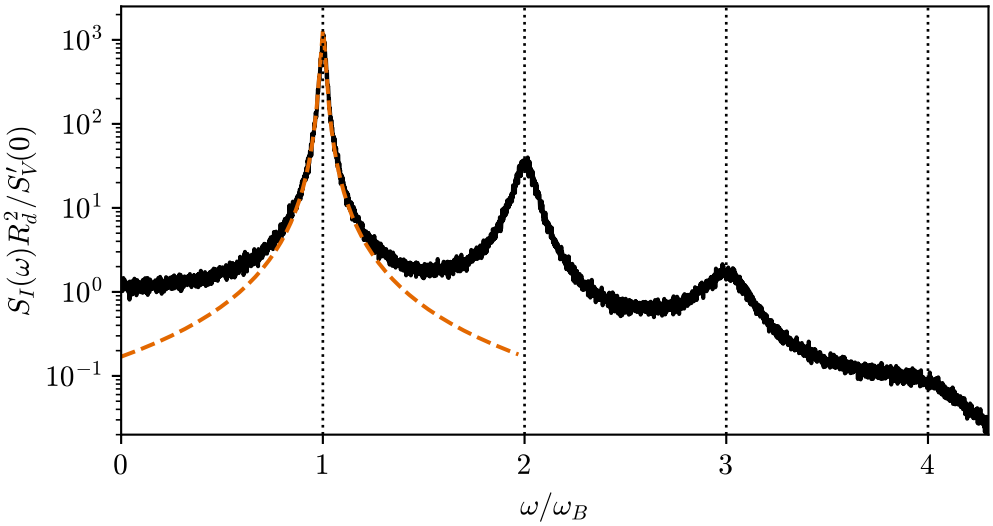

Figure 3.3: Current spectral density of a DC-biased phase-slip junction under the influence of thermal, white noise for $V_{0,\mathrm{dc}} = 1.4V_c$ and $\gamma_0 = 5 \times 10^{-3}$. The black, solid line shows the numerical solution of Eq. (3.15). The orange, dashed line displays the analytical result for the first peak in Eq. (3.14). Due to thermal noise, the spectrum exhibits Lorenzian peaks of finite width at integer multiples of ω_B.

its average value $\omega_B \mapsto \omega_B + \pi\xi_I(t)/e$. This so-called phase- or frequency-noise causes the spectra of the total current to exhibit peaks of finite width at integer multiples of ω_B instead of the δ-shaped singularities predicted by Eq. (2.9) [15]. As we are only interested in the first dual Shapiro step, we are going to focus on the linewidth Γ_1 of the first peak at ω_B. As before, we assume the case of small fluctuations, when the linewidth is small in the sense $\Gamma_1 \ll \omega_B$.

Due to the definition of the spectral density in Eq. (3.3), we can relate the spectral density of the current $I(t)$ to the spectral density of the normalized charge $N(t)$ via the relation between their Fourier transforms $N(\omega) = i\pi I(\omega)/e\omega$. We find

$$S_N(\omega) = \left|\frac{\pi}{e\omega}\right|^2 S_I(\omega). \tag{3.12}$$

Since the phase fluctuations are growing as ω^{-2} as $\omega \to 0$, the lower frequency components of $I(t)$ cause the largest phase perturbations and are, thus, responsible for the fluctuations around the first dual Shapiro step and the linewidth Γ_1 [15].

For wide-band noise, we can take the spectral density $S_I(\omega)$ to be constant in the relevant regime $0 \leq \omega \leq \Gamma_1$, far away from the first peak at ω_B. The

linewidth Γ_1 can be determined by calculating the spectral density of the single oscillation $I_1(t) = 2|I_1|\cos[\omega_B t + \int_{-\infty}^{t} dt' \pi \xi_I(t')/e + \varphi_1]$ [15]. Here, the amplitude I_1 is given by Eq. (2.9) and φ_1 is an arbitrary phase. The auto-correlation of $I_1(t)$ is given by

$$\begin{aligned}\langle\langle I_1(t) I_1(0)\rangle\rangle &= |I_1|^2 \left\langle\left\langle \exp\left[i\omega_B t + i\frac{\pi}{e}\int_0^t dt' \xi_I(t')\right]\right\rangle\right\rangle + \text{c.c.} \\ &= 2|I_1|^2 \cos(\omega_B t) \exp\left[-\frac{\pi^2}{2e^2}\int_0^t dt' \int_0^t dt'' \underbrace{\langle\langle \xi_I(t')\xi_I(t'')\rangle\rangle}_{S_I(0)\delta(t'-t'')}\right] \\ &= 2|I_1|^2 \cos(\omega_B t) \exp\left[-\frac{\pi^2}{2e^2} S_I(0)|t|\right]. \end{aligned} \tag{3.13}$$

The spectral density is the Fourier transform of this auto-correlation and has a Lorentzian line shape

$$S_{I_1}(\omega) = |I_1|^2 \left[\frac{2\Gamma_1}{(\omega-\omega_B)^2 + \Gamma_1^2} + \frac{2\Gamma_1}{(\omega+\omega_B)^2+\Gamma_1^2}\right], \quad \Gamma_1 = \frac{\pi^2}{2e^2} S_I(0). \tag{3.14}$$

The remaining task is to relate $S_I(0)$ to the voltage spectral density $S_V(0) = 2Rk_BT$. In order to find such a relation, we add fluctuations to Eq. (2.6)

$$\frac{\dot{N}_{\mathrm{dc,f}}}{\omega_R} + \sin(N_{\mathrm{dc,f}}) = v_{0,\mathrm{dc}} + \frac{\xi_V(t)}{V_c}. \tag{3.15}$$

Here, compared to Eq. (3.8), we can no longer set $v_{0,\mathrm{dc}} = 0$ and linearize the sine-function as we are interested in the influence of noise away from the Coulomb blockade step. Assuming the fluctuations are small, we can make the ansatz $N_{\mathrm{dc,f}} = N_{\mathrm{dc}} + N_f$ and linearize the previous equation with respect to small phase fluctuations N_f [15]. We obtain an equation similar to Eq. (2.12)

$$\frac{\dot{N}_f}{\omega_R} + \cos(N_{\mathrm{dc}}) N_f = \frac{\xi_V(t)}{V_c}. \tag{3.16}$$

Thus, we can follow similar steps as in Eq. (2.13) to solve this differential equation. For the fluctuating current $I_f = e\dot{N}_f/\pi$, we find

$$I_f(t) = \frac{1}{R}\left[\dot{I}_{\mathrm{dc}}(t) \int_{-\infty}^{t} dt' \frac{\xi_V(t')}{I_{\mathrm{dc}}(t')} + \xi_V(t)\right]. \tag{3.17}$$

Since we want to relate the current spectral density to the voltage spectral density, we insert voltage fluctuations at a single frequency $\xi_V(t) = \mathrm{Re}(V_\omega e^{-i\omega t})$

into the equation for I_f. Then, we use the Fourier decomposition of I_{dc} in Eq. (2.9) to obtain a relation between the Fourier components of the current I_ω and the voltage V_ω

$$I_\omega = \sum_{k=-\infty}^{\infty} Z_k^{-1}(\omega - k\omega_B) V_{\omega - k\omega_B}. \tag{3.18}$$

where the impedance $Z_k(\omega)$ depends on the position on the IV-curve and the system parameters via

$$\begin{aligned} RZ_k^{-1}(\omega) &= \delta_{k,0} + \frac{k\,\omega_R\, v_{0,\mathrm{dc}}}{i^k\,\omega\,(i_0 + v_{0,\mathrm{dc}})^{|k|}} e^{it_0 k\omega_B} \\ &- \frac{1}{2i^k}\left[\frac{(k-1)\,\omega_R}{(\omega+\omega_B)(i_0+v_{0,\mathrm{dc}})^{|k-1|}} + \frac{(k+1)\,\omega_R}{(\omega-\omega_B)(i_0+v_{0,\mathrm{dc}})^{|k+1|}}\right] e^{it_0 k\omega_B}. \end{aligned} \tag{3.19}$$

In accordance with the definition of the spectral density, Eq. (3.18) yields the general expression

$$S_I(\omega) = \sum_{k=-\infty}^{\infty} |Z_k^{-1}(\omega - k\omega_B)|^2 S_V(\omega - k\omega_B). \tag{3.20}$$

For $\omega \ll \omega_B$ and $S_V(\omega) = 2Rk_BT$, we can perform the sum over k explicitly and obtain

$$S_I(0) = \frac{S_V'(0)}{R_d^2}, \qquad S_V'(0) = 2Rk_BT\left(1 + \frac{1}{2v_{0,\mathrm{dc}}^2}\right), \tag{3.21}$$

where R_d is the previously defined differential resistance that depends on the position on the IV-curve [15]. Using this result, we can express the linewidth Γ_1 as

$$\Gamma_1 = \pi \frac{1 + 2v_{0,\mathrm{dc}}^2}{v_{0,\mathrm{dc}}^2 - 1} \frac{R_Q}{R} \frac{k_BT}{\hbar}. \tag{3.22}$$

As expected, the linewidth increases with rising temperature and decreases for large resistances.

At this point, we are in the position to obtain an expression for the variance of δN in Eq. (3.10) and, thus, the effective noise parameter γ_1. With that, we predict the point at which the dual Shapiro steps are being washed out by thermal fluctuations. Intuitively, this point is determined by comparing the linewidth Γ_1 to the frequency scale $\omega_1 = \pi\Delta V/2eR_d$ associated with the height

of the step. For $\Gamma_1 \gtrsim \omega_1$, the steps are being washed out. More rigorously, we can calculate the variance of δN analogously to the calculation for the Coulomb blockade step using the effective noise spectral density $S'_V(0)$ that we calculated in Eq. (3.21). Both derivations obtain the same result

$$\langle\langle \delta N^2 \rangle\rangle = 2\pi \frac{k_B T}{e\Delta V} \underbrace{\frac{R}{R_d}\left(1 + \frac{1}{2v_S^2}\right)}_{\gtrsim 1} = \frac{\Gamma_1}{\omega_1} = \gamma_1, \tag{3.23}$$

where $v_S = [(\omega_0/\omega_R)^2 + 1]^{1/2}$ corresponds to the normalized step position. All our results are valid for a small AC-voltage $V_{\mathrm{ac}} \ll V_c$.

We conclude that we essentially need to compare the height of the step ΔV to the temperature scale $k_B T/e$ to determine whether the step is washed out. In the regime $V_{\mathrm{ac}} \ll V_c$, the noise parameter γ_1 is much larger than γ_0. Therefore, the washing out of the first dual Shapiro step takes place at much smaller temperature than the washing out of the Coulomb blockade step [15].

However, we can be even more precise by including the full formula for the noise parameter γ_1 in Eq. (3.23). This can be done by defining a renormalized step height $\Delta V'$ with

$$\Delta V' = \frac{R_d}{R}\left(1 + \frac{1}{2v_S^2}\right)^{-1} \Delta V = \frac{\sqrt{v_S^2 - 1}}{v_S + 1/2v_S}\Delta V. \tag{3.24}$$

Instead of comparing the actual step height ΔV to the temperature scale $k_B T/e$, one can use this effective step height $\Delta V'$ for a more precise result. A comparison between ΔV and $\Delta V'$ can be found in Fig. 3.4. Due to the renormalization, small ratios ω_0/ω_R become unfavourable for the measurement of dual Shapiro steps and a clear maximum step height develops at $\omega_0 \approx \omega_R$.

Our results suggest that dual Shapiro steps smaller than $\Delta V' \simeq V_c$ ($V_c \simeq 10\,\mu\mathrm{V}$) are suppressed at a temperature of $T \simeq 20\,\mathrm{mK}$. This would imply that for a resistor at a realistic temperature of $T \simeq 100\,\mathrm{mK}$ even the measurement of Coulomb blockade is not possible. However, effective filtering methods can be employed to significantly lower the thermal noise of off-chip resistors. This has been repeatedly demonstrated in previous Coulomb blockade measurements [4, 16, 20, 21].

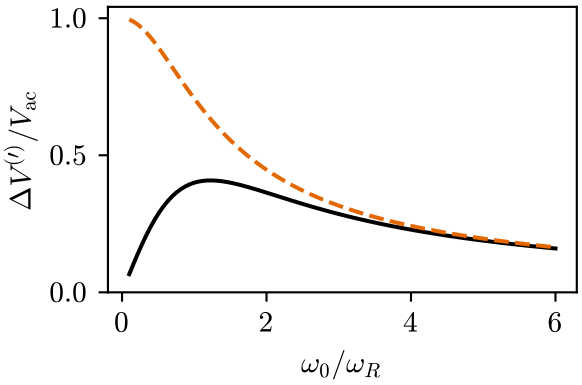

Figure 3.4: Comparison between the renormalized dual Shapiro step height in Eq. (3.24) (black, solid) and the analytical result at $T = 0$ in Eq. (2.16) (orange, dashed). In presence of thermal noise, small ratios ω_0/ω_R become unfavourable for the measurement of dual Shapiro steps. A clear maximum step height develops at $\omega_0 \approx \omega_R$.

3.3 Extension to quantum noise

In the previous sections, we focused on classical Johnson-Nyquist noise. However, for temperature $k_B T \lesssim \hbar\omega_B$, quantum fluctuations start to play an important role in the noise characteristic. Here, the classical Johnson-Nyquist noise should be replaced by the more general quantum noise. The corresponding, symmetrized spectral density is given by [22]

$$S_V(\omega) = R\hbar\omega \coth\left(\frac{\hbar\omega}{2k_B T}\right), \tag{3.25}$$

which simplifies to the Johnson-Nyquist formula in the limit $k_B T \gg \hbar\omega$.

In order to include quantum fluctuations in the previous calculation of the effective noise parameter γ_1, we have to reevaluate Eq. (3.20) using the spectral density for quantum noise in Eq. (3.25). For $\omega \ll \omega_B$, we obtain [15]

$$S_I(0) = \frac{S'_V(0)}{R_d^2}, \qquad S'_V(0) = \underbrace{2Rk_B T}_{S_V(0)} + \frac{1}{2v_{0,\mathrm{dc}}^2} \underbrace{R\hbar\omega_B \coth\left(\frac{\hbar\omega_B}{2k_B T}\right)}_{S_V(\omega_B)}. \tag{3.26}$$

We can clearly see that not only the quantum fluctuations at zero frequency contribute to $S_I(0)$ and, thus, the linewidth Γ_1, but also fluctuations around the Bloch frequency. Therefore, the adapted current spectral density remains finite for $T \to 0$ with a value of $S_I^*(0) = \hbar\omega_B/2i_0^2 R$. This special property is due to the periodic potential of the phase-slip junction that allows a DC-drive to cause an AC-response, thus, enabling the system to dissipate the excess en-

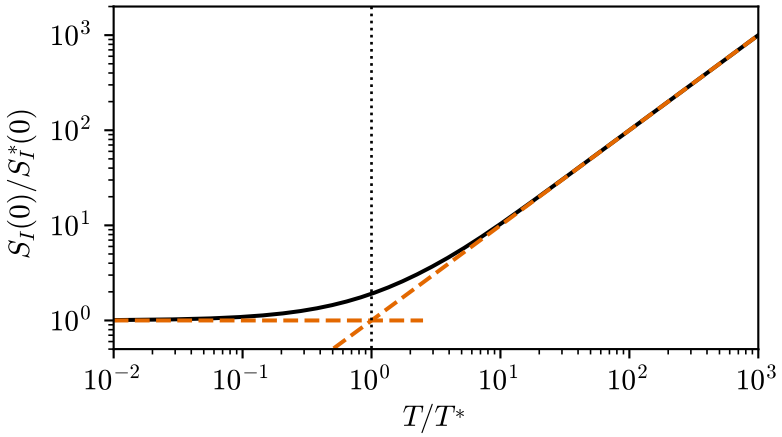

Figure 3.5: Zero frequency current spectral density $S_I(0)$ as a function of temperature T in presence of quantum noise (black, solid). The orange, dashed lines correspond to the Johnson-Nyquist approximation at high temperature as well as the zero temperature limit. At $T = T^*$, both approximations provide the same result.

ergy of the drive at finite frequency. For $k_B T \gg \hbar\omega_B$, we obtain the original, classical result in Eq. (3.21).

The adapted current spectral density is displayed in Fig. 3.5 together with the low temperature limit and the classical high temperature approximation. The temperature T^* marks the transition between the low and high temperature regime. It can be approximated by the intersection of both approximations with the result

$$T^* = \frac{1}{4v_{0,\mathrm{dc}} + 2} \frac{\hbar\omega_B}{k_B}. \tag{3.27}$$

We can conclude that the calculations in the classical, white noise limit are valid for temperature $T > T^*$. For temperature $T < T^*$, quantum fluctuations become relevant and the resulting noise is equivalent to the classical noise at $T = T^*$. In this regime, we, thus, have to substitute the physical temperature of the system for the effective noise temperature T^* of the Bloch oscillations [23].

The corresponding effective noise parameter at zero temperature is given by

$$\gamma_1^* = \frac{\pi}{2v_S\sqrt{v_S^2 - 1}} \frac{\hbar\omega_B}{e\Delta V}. \tag{3.28}$$

This result renders filtering below the effective noise temperature useless. For a realistic drive frequency $\omega_0/2\pi \simeq 5\,\mathrm{GHz}$ and $\omega_0 \simeq \omega_R$, we obtain an effective

noise temperature $T^* \simeq 20\,\mathrm{mK}$ which is usually below the temperature of a typical off-chip resistor discussed in the previous section. Furthermore, for $\Delta V \simeq V_c$, we obtain an effective zero temperature noise parameter

$$\gamma_1^* \simeq \frac{\pi}{v_S}\frac{R_Q}{R}. \tag{3.29}$$

Thus, for $R \gg R_Q$, the influence of the effective noise temperature of the Bloch oscillations is negligible and a classical treatment of the noise is sufficient.

Chapter 4

Screening from parasitic capacitance

4.1 Need for superinductance

Up to this point, we have considered the ideal situation where the voltage source together with the large resistance R constitutes an almost ideal current source with value $V(t)/R$. However, in a realistic situation, an unwanted parasitic capacitance C_p tends to shunt the Josephson junction destroying the perfect current bias, see Fig. 4.1(a). Such a parasitic capacitance is either due to direct coupling between the leads caused by insufficient separation or due to indirect coupling between the leads through a common ground plane. The total parasitic capacitance is usually of the order of 1 pF [6]. Thus, the associated charging energy $E_{C_p} = e^2/2C_p$ is very small compared to the charging energy E_C of the Josephson junction. Since the charging energies of parallel capacitances add up inversely, the total charging energy is of the order of E_{C_p}. As we have shown in Eq. (2.4), this leads to an exponentially small phase-slip energy which in turn causes an exponential suppression of the amplitude of the Bloch oscillation.

An intuitive remedy for this detrimental effect is a large on-chip resistance, $R \gtrsim R_Q$ which protects the junction from the influence of the parasitic capacitance. However, placing this resistance close to the junction causes excessive heating. As demonstrated in the previous chapter, this leads to the washing out of the dual Shapiro steps [4]. It has been argued that the complementary requirements — large resistance for good current biasing and small resistance for small heating — are irreconcilable [6]. Instead, a superinductance L with characteristic impedance $Z = \sqrt{L/C_p} \geq R_Q$ has been proposed as a reactive alternative in order to screen the junction from the influence of the parasitic

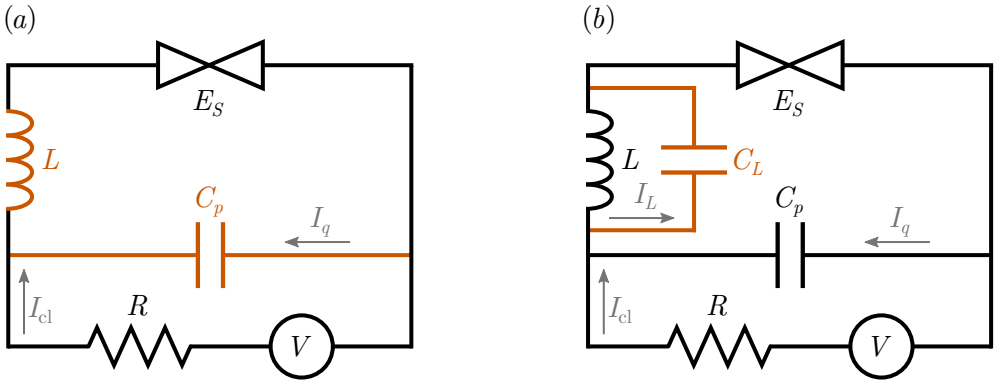

Figure 4.1: (a) Realistic setup of a phase-slip junction shunted by an unwanted, parasitic, off-chip capacitance. This circuit is an extension of the ideal circuit in Fig. 2.2. The parasitic capacitance C_p causes the part $-I_q$ of the current to flow past the junction. To remedy this unwanted effect, an additional on-chip superinductance L is introduced. (b) Extended realistic setup with an additional capacitance C_L parallel to the inductance. This capacitance causes the part I_L of the current to flow past the superinductance.

capacitance [24–26].

However, as the system is constantly driven, the energy still has to be dissipated at some point. In Ref. [6], the authors have proposed to implement the driving as well as the dissipation by a microwave transmission line. Here, we treat an alternative setup where we combine the idea of the superinductance to protect against parasitic capacitance in the inner current loop with a resistance in series with the voltage source. The key point is that the resistance does not have to be close to the Josephson junction as the superinductance serves to protect against the parasitic capacitance. Rather, the task of the resistance is to turn the voltage source into a current source and to dissipate excess energy so that the system may settle into a stationary state.

The results obtained in this and the following chapter are discussed in the context of a paper in Ref. [27].

4.2 System parametrization of adapted circuit

The system, we propose in order to observe dual Shapiro steps, is given by Fig. 4.1(a). In this setup, an inductance L serves to protect against the parasitic capacitance C_p. We denote the current in the outer loop by I_{cl}. The current in this loop is driven by the voltage source and it is stabilized by the presence

of a resistance R. The current in the inner loop, denoted by I_q, flows without dissipation. As before, the step to a quantum description of the problem is performed by introducing the loop charge operators $\hat{Q}_{\mathrm{cl}[q]} = \int_{-\infty}^{t} dt' \, \hat{I}_{\mathrm{cl}[q]}(t')$ which denote the charge that has flown in the individual loops up to a time t [8]. Kirchhoff's voltage law then demands that

$$R\dot{\hat{Q}}_{\mathrm{cl}} = V(t) + \frac{\hat{Q}_q}{C_p}, \tag{4.1}$$

$$L(\ddot{\hat{Q}}_{\mathrm{cl}} + \ddot{\hat{Q}}_q) + V_c \sin\left[\frac{\pi}{e}(\hat{Q}_{\mathrm{cl}} + \hat{Q}_q)\right] + \frac{\hat{Q}_q}{C_p} = 0. \tag{4.2}$$

Since the influence of noise has already been discussed in Ch. 3, we include only the noiseless, classical part of the voltage source.

As discussed in Sec. 2.2, in the regime $R \gg R_Q$, the quantum fluctuations of $\hat{Q}_{\mathrm{cl}}$ are suppressed far below $2e$ [13] and we can replace $\hat{Q}_{\mathrm{cl}}$ by its quantum-mechanical expectation value $Q_{\mathrm{cl}} = \langle \hat{Q}_{\mathrm{cl}} \rangle$. Thus, the current I_{cl} can be measured via the voltage drop over the resistance R. On the other hand, the fluctuations of $\hat{Q}_q$ are suppressed by the characteristic impedance $Z = \sqrt{L/C_p}$. The motion of $\hat{Q}_q$ is given by Eq. (4.2). This equation describes a non-dissipative dynamics of $\hat{Q}_q$ and can, therefore, be replaced by a Schrödinger equation. The explicit form of the Hamiltonian that generates the equation of motion for $\hat{Q}_q$ is given by

$$\hat{H} = \frac{\hat{\Phi}_q^2}{2L} + \frac{\hat{Q}_q^2}{2C_p} + L\hat{Q}_q\ddot{Q}_{\mathrm{cl}} - \frac{eV_c}{\pi}\cos\left[\frac{\pi}{e}(\hat{Q}_q + Q_{\mathrm{cl}})\right], \tag{4.3}$$

where $\hat{\Phi}_q$ is the canonically conjugate variable of $\hat{Q}_q$ with $[\hat{Q}_q, \hat{\Phi}_q] = i\hbar$. The equation of motion in Eq. (4.2) can be obtained via the Hamilton formalism with $L\ddot{\hat{Q}}_q = \dot{\hat{\Phi}}_q = [\hat{\Phi}_q, \hat{H}]/i\hbar$. Note, that this Hamiltonian is time-dependent, where the time-dependence is parametrized by Q_{cl}. Thus, the problem reduces to finding the solution of the time-dependent Schrödinger equation $i\hbar\partial_t\psi(Q_q; Q_{\mathrm{cl}}, t) = \hat{H}\psi(Q_q; Q_{\mathrm{cl}}, t)$ for the quantum loop charge coupled to the equation of motion

$$R\dot{Q}_{\mathrm{cl}} = \frac{\langle\psi|\hat{Q}_q|\psi\rangle}{C_p} + V(t) \tag{4.4}$$

for the classical loop charge.

The dynamics of the circuit are governed by three distinct rates: the plasma frequency of the quantum charge $\omega_q = 1/\sqrt{LC_p}$, the plasma frequency of the

classical charge $\omega_{\mathrm{cl}} = 1/\sqrt{LC_S}$, and the RC-rate $\omega_R = 1/RC_S$ with which the motion is damped. The ratio $\omega_{\mathrm{cl}}/\omega_R$ is the quality factor of the classical charge dynamics and measures the relative importance of the first- with respect to the second-order time derivative of Q_{cl}. For $\omega_R > \omega_{\mathrm{cl}}$, the system can show hysteretic behavior, which makes it very unfavorable for the accurate observation of dual Shapiro steps. In Ch. 5, we, therefore, focus on the overdamped regime with $\omega_{\mathrm{cl}} \gg \omega_R$.

4.3 Influence of capacitance parallel to inductance

In a realistic setup, every inductance L has a parallel capacitance C_L, as displayed in Fig. 4.1(b). This parallel capacitance is usually of the order of 1 fF and, thus, much smaller than the parasitic capacitance. Additionally, it does not shunt part of the current injected by the source and, therefore, does not cause the same detrimental effects as the parasitic capacitance. Thus, we have chosen to neglect it in the previous section of this chapter and continue to do so in most parts of the following chapter. Nevertheless, we are going to give a short insight into the influence of the parallel capacitance in this section.

Building on the description of the system introduced in the previous section, we are going to derive a new Hamiltonian for the quantum loop, including the additional capacitance. Introducing a third loop charge Q_L for the additional loop, the Lagrangian for the quantum loop is given by

$$\mathcal{L} = \frac{L}{2}(\dot{Q}_q + \dot{Q}_{\mathrm{cl}} - \dot{Q}_L)^2 - \frac{Q_q^2}{2C_p} + \frac{eV_c}{\pi}\cos\left[\frac{\pi}{e}(Q_q + Q_{\mathrm{cl}})\right] - \frac{Q_L^2}{2C_L}, \tag{4.5}$$

where Q_{cl} remains a classical variable analogously to the previous section. Introducing the charges $Q_q' = Q_q - Q_L$ and $Q_q'' = (Q_q + Q_L)/2$, it is obvious that the state of the system depends only on the current $\dot{Q}_q'$ through the inductance and not on the separate currents through the capacitive branches. The fact that the Lagrangian does not depend on $\dot{Q}_q''$ also means that the Euler-Lagrange equation $\partial\mathcal{L}/\partial Q_q'' = d(\partial\mathcal{L}/\partial\dot{Q}_q'')/dt = 0$ yields the purely algebraic constraint

$$Q_q'' = -V_c\frac{C_pC_L}{C_p + C_L}\sin\left[\frac{\pi}{e}\left(\frac{Q_q'}{2} + Q_q'' + Q_{\mathrm{cl}}\right)\right] + \frac{C_p - C_L}{C_p + C_L}\frac{Q_q'}{2}. \tag{4.6}$$

For $(C_L/C_S)[C_p/(C_p+C_L)] \simeq C_L/C_S < 1$, this equation has one unique solution. In this regime, Eq. (4.6) can be solved to obtain

$$Q_q'' = \frac{C_p - C_L}{C_p + C_L}\frac{Q_q'}{2} - \frac{e}{\pi}\frac{C_L}{C_S}\frac{C_p}{C_p + C_L}\sin\left[\frac{\pi}{e}\left(\frac{C_p}{C_p + C_L}Q_q' + Q_{\mathrm{cl}}\right)\right], \tag{4.7}$$

valid to first order in C_L/C_S. However, for the following derivation, we are going to take only the lowest order term into account since we are interested in the leading order effect of the parallel capacitance.

After reinserting the solution for Q_q'' into the Lagrangian and performing the Legendre transformation, we obtain the Hamiltonian

$$\hat{H} = \frac{\hat{\Phi}_q'^2}{2L} + \frac{\hat{Q}_q'^2}{2(C_p + C_L)} + L\hat{Q}_q'\ddot{Q}_{\mathrm{cl}} - \frac{eV_c}{\pi}\cos\left[\frac{\pi}{e}\left(\frac{C_p}{C_p + C_L}\hat{Q}_q' + Q_{\mathrm{cl}}\right)\right], \tag{4.8}$$

where $\hat{\Phi}_q'$ is the canonically conjugate variable of $\hat{Q}_q'$ with $[\hat{Q}_q', \hat{\Phi}_q'] = i\hbar$. In the last step, we additionally applied the gauge transformation $\psi \mapsto e^{iL\dot{Q}_{\mathrm{cl}}\hat{Q}_q'/\hbar}\psi$ in order to obtain a Hamiltonian of a similar form as Eq. (4.3). Analogously to the previous section, the problem reduces to finding the solution of the time-dependent Schrödinger equation $i\hbar\partial_t\psi(Q_q'; Q_{\mathrm{cl}}, t) = \hat{H}\psi(Q_q'; Q_{\mathrm{cl}}, t)$ for the quantum loop charge coupled to the equation of motion

$$R\dot{Q}_{\mathrm{cl}} = \frac{\langle\psi|\hat{Q}_q'/2 + \hat{Q}_q''|\psi\rangle}{C_p} + V(t), \tag{4.9}$$

for the classical loop charge. Here, $\hat{Q}_q''$ depends on $\hat{Q}_q'$ via Eq. (4.7).

Compared to the previous section, we find that due to the parallel capacitance of the inductance the plasma frequency of the quantum charge is modified to $\omega_q' = 1/\sqrt{L(C_p + C_L)}$. In addition, the periodicity of the cosine potential of the phase-slip junction is slightly modified by the factor $(C_p + C_L)/C_p$. We continue to discuss the influence of these adjustments within the framework of the ground state approximation in Sec. 5.2.

Chapter 5

Analysis of dual Shapiro step height

5.1 High impedance regime

In this chapter, we focus on calculating the dual Shapiro step height in presence of the parasitic capacitance and the superinductance. First, we analyze the system in the regime of large characteristic impedance, $Z \gg R_Q$. In this case, the charge $\hat{Q}_q$ as well as its fluctuations in the parasitic loop remain small compared to $2e$ [13]. This allows us to linearize Eq. (4.2) and treat $\hat{Q}_q$ classically. Next, we insert the linearized expression for Q_q into Eq. (4.1) for the classical loop charge. In the overdamped regime, we can additionally neglect the second order time derivatives with respect to the first order time derivative. We obtain a differential equation for Q_{cl}

$$R\dot{Q}_{\mathrm{cl}} + \frac{V_c \sin(\pi Q_{\mathrm{cl}}/e)}{1 + (C_p/C_S)\cos(\pi Q_{\mathrm{cl}}/e)} = V(t). \tag{5.1}$$

By expanding this equation up to second order in small C_p/C_S, we obtain

$$\frac{\dot{N}}{\omega_R} + \sin(N) - \frac{C_p}{2C_S}\sin(2N) + \frac{C_p^2}{4C_S^2}\left[\sin(N) + \sin(3N)\right] = v(t), \tag{5.2}$$

where $v(t) = V(t)/V_c$ is the normalized voltage and $N = \pi Q_{\mathrm{cl}}/e$ the normalized charge in the classical loop. For vanishing C_p, this reduces to the ideal model which we already discussed in Ch. 2.

In this section, we want to obtain the step height for finite C_p up to second order in small C_p/C_S. Analogously to the calculation in Ch. 2, we first need

to find a solution to Eq. (5.2) without an AC-drive. Therefore, we make the ansatz $N_{\mathrm{dc}} = N_{\mathrm{dc}}^{(0)} + (C_p/2C_S)N_{\mathrm{dc}}^{(1)} + (C_p/2C_S)^2 N_{\mathrm{dc}}^{(2)}$ and we also expand the DC-drive $v_{0,\mathrm{dc}} = v_{0,\mathrm{dc}}^{(0)} + (C_p/2C_S)v_{0,\mathrm{dc}}^{(1)} + (C_p/2C_S)^2 v_{0,\mathrm{dc}}^{(2)}$ in the same way. The result for $N_{\mathrm{dc}}^{(0)}$ can be found in Eq. (2.7). In order to obtain the higher order contributions, we separate Eq. (5.2) and arrive at the expression

$$\int dN_{\mathrm{dc}} \Bigg\{ v_{0,\mathrm{dc}}^{(0)} - \sin(N_{\mathrm{dc}}) + \frac{C_p}{2C_S}\left[v_{0,\mathrm{dc}}^{(1)} + \sin(2N_{\mathrm{dc}}) \right] + \frac{C_p^2}{4C_S^2}\left[v_{0,\mathrm{dc}}^{(2)} - \sin(N_{\mathrm{dc}}) - \sin(3N_{\mathrm{dc}}) \right] \Bigg\}^{-1} = \omega_R (t - t_0). \tag{5.3}$$

Now, we expand the integrand up to second order in small C_p/C_S and perform the resulting integrals. Then, we can insert the expansion for N_{dc} and sort the expression in orders of C_p/C_S. While the zeroth order term leads to Eq. (2.7), solving the higher order terms in succession results in analytical expressions for $N_{\mathrm{dc}}^{(1)}$ and $N_{\mathrm{dc}}^{(2)}$. Since both expressions are quite involved, we refrain from writing them down here.

As a next step, we choose $v_{0,\mathrm{dc}}^{(1)}$ and $v_{0,\mathrm{dc}}^{(2)}$ in such a way that $\overline{\dot{N}_{\mathrm{dc}}^{(1)}}, \overline{\dot{N}_{\mathrm{dc}}^{(2)}} = 0$. This way, higher orders will not contribute to the average current. Our former relation $i_0 = \overline{I}_{\mathrm{dc}} R/V_c = [(v_{0,\mathrm{dc}}^{(0)})^2 - 1]^{1/2}$, thus, remains valid throughout the calculation. By applying the condition to our analytical results, we obtain

$$v_{0,\mathrm{dc}}^{(1)} = 0, \tag{5.4}$$

$$v_{0,\mathrm{dc}}^{(2)} = 6v_{0,\mathrm{dc}}^{(0)} - 4\left(v_{0,\mathrm{dc}}^{(0)}\right)^3 + 4\left[\left(v_{0,\mathrm{dc}}^{(0)}\right)^2 - 1\right]^{3/2}. \tag{5.5}$$

Therefore, the first step at $I_S = e\omega_0/\pi$ is centered around the voltage V_S given by

$$V_S = V_S^{(0)} + \frac{C_p^2}{4C_S^2}\, v_{0,\mathrm{dc}}^{(2)}\, V_c, \tag{5.6}$$

with $V_S^{(0)} = V_c v_{0,\mathrm{dc}}^{(0)}$ the step position in absence of the parasitic capacitance. In order to calculate the step height, we need to use Eq. (2.14) again which remains valid in the case $C_p \neq 0$. Going through the same steps as in Sec. 2.3, we finally obtain the height of the first step

$$\Delta V = \Delta V^{(0)} + \frac{C_p^2}{4C_S^2}\left\{ 1 + \frac{29}{96}\left(v_{0,\mathrm{dc}}^{(0)}\right)^{-2} + \mathcal{O}\left[\left(v_{0,\mathrm{dc}}^{(0)}\right)^{-3}\right] \right\} \frac{V_{\mathrm{ac}}}{v_{0,\mathrm{dc}}^{(0)}}, \tag{5.7}$$

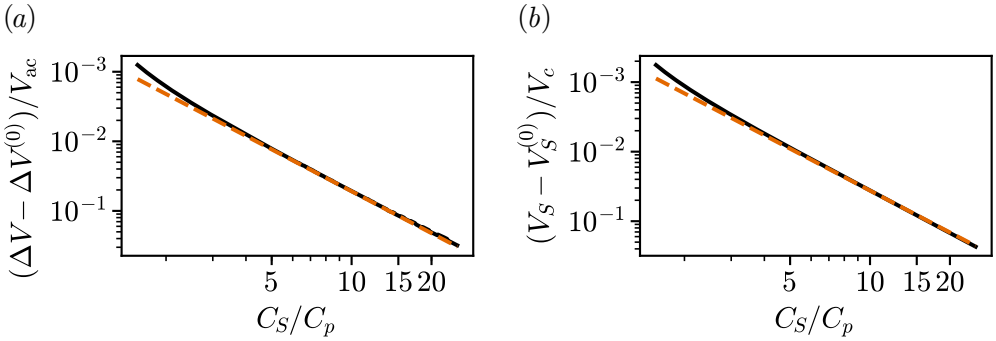

Figure 5.1: (a), (b) Logarithmic plot of the dual Shapiro step height and position in the high impedance regime as a function of the parasitic capacitance C_p. The black, solid line shows the numerical solution of Eq. (5.1) for $V_{\rm ac} = 0.1V_c$. The orange, dashed line corresponds to the analytical results in Eqs. (5.7) and (5.6). For large C_S/C_p, the analytical results approximate the numerical solution very well.

with $\Delta V^{(0)} = V_{\rm ac}/v^{(0)}_{0,\rm dc}$ the step height in absence of the parasitic capacitance. The result is valid to leading order in $V_{\rm ac}/V_c$ and C_p/C_S. We conclude that in the high impedance regime the presence of a small parasitic capacitance increases the height of the dual Shapiro step.

5.2 Ground state approximation

Experimentally more relevant is the regime $Z \simeq R_Q$. In order to obtain analytical results in this regime, we assume the plasma frequency of the quantum charge ω_q to be large. In particular, we demand that the parasitic capacitance is small enough such that the relations $\omega_q \gg \omega_0$ and $\omega_q \gg eV_c/\hbar \simeq \omega_R R/R_Q$ hold. Under these conditions, the quantum loop charge stays in the ground state of the Hamiltonian in Eq. (4.3) during the course of the evolution, given the system is initially at sufficiently low temperatures with $k_B T \ll \hbar\omega_q$. Specifically, as $\omega_q \gg \omega_0$ and $\hbar\omega_q \gg eV_c$, we can neglect the last two terms in Eq. (4.3). Then, the ground state wave function is that of a harmonic oscillator and is given by

$$\psi_0(Q_q, Q_{\rm cl}, t) = \frac{Z^{1/4}}{\pi^{1/4}\hbar^{1/4}} e^{-(Z/2\hbar)Q_q^2 - i\omega_q t/2}. \tag{5.8}$$

Next, we need to approximate the expectation value of $\hat{Q}_q/C_p$. Since we assume C_p to be a small parameter in our expansion we can not simply take the expectation value of $\hat{Q}_q$ in the ground state and divide the result by C_p. Instead

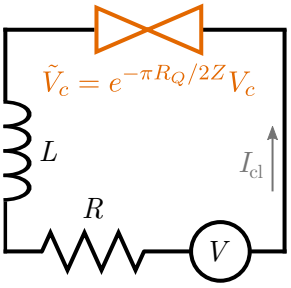

Figure 5.2: Circuit corresponding to the ground state approximation in Eq. (5.11). Compared to the original circuit in Fig. 4.1(a), the parasitic capacitance has vanished as a circuit element. Instead the influence of the parasitic capacitance is incorporated via a renormalization of the critical voltage $\tilde{V}_c = e^{-\pi R_Q/2Z} V_c$.

we express $\hat{Q}_q/C_p$ in terms of the commutator $[\hat{H}, \hat{\Phi}_q]$

$$\frac{\hat{Q}_q}{C_p} = \frac{[\hat{H}, \hat{\Phi}_q]}{i\hbar} - L\ddot{Q}_{\mathrm{cl}} - V_c \sin\left[\frac{\pi}{e}(\hat{Q}_q + Q_{\mathrm{cl}})\right]. \tag{5.9}$$

Within our approximation, the Hamiltonian describes only the harmonic oscillator. Thus, the expectation value of the commutator in the ground state of this harmonic oscillator is zero and we only have to calculate the expectation value of

$$\left\langle \psi_0 \right| \sin\left[\frac{\pi}{e}(\hat{Q}_q + Q_{\mathrm{cl}})\right] \left| \psi_0 \right\rangle = e^{-\pi R_Q/2Z} \sin\left(\frac{\pi}{e} Q_{\mathrm{cl}}\right). \tag{5.10}$$

If we insert both results in Eq. (4.4), the equation of motion of the classical charge reduces to

$$L\ddot{Q}_{\mathrm{cl}} + R\dot{Q}_{\mathrm{cl}} + e^{-\pi R_Q/2Z} V_c \sin\left(\frac{\pi}{e} Q_{\mathrm{cl}}\right) = V(t), \tag{5.11}$$

valid to lowest order in $eV_c/\hbar\omega_q$ and ω_0/ω_q.

This equation corresponds to the circuit in Fig. 5.2. Here, the sole effect of the parasitic capacitance is to reduce the critical voltage of the phase-slip junction V_c by a factor $e^{-\pi R_Q/2Z}$. This implies that the effect of the parasitic capacitance is shielded by the inductance as long as the characteristic impedance Z is larger than $\pi R_Q/2 \approx 10\,\mathrm{k}\Omega$. The factor is caused by charge fluctuations. As indicated by Eq. (4.4), the width of the wave function in charge space is given by $\Delta Q_q = \sqrt{\hbar/2Z}$. The periodic potential due to the phase-slip junction is $2e$ periodic. This potential term is treated as a perturbation to the harmonic oscillator. The perturbation only depends on the average charge flowing through the junction, if the width of the wave function is of the order of or smaller than the periodicity of the potential. The ratio $\Delta Q_q/2e \simeq \sqrt{R_Q/Z}$, thus, determines whether the classical charge 'feels' the periodic potential, which is responsible for the emergence of Bloch oscillations.

Following similar steps, we can also derive an effective equation of motion in the presence of the small capacitance parallel to the inductance as discussed in Sec. 4.3. We insert Eq. (4.7) into Eq. (4.9) and calculate the resulting expectation value analogously to Eq. (5.9) using the adjusted Hamiltonian in Eq. (4.8). To lowest order in C_L/C_S, we obtain an equation identical to Eq. (5.11) with a renormalized impedance

$$Z' = Z\left(\frac{C_p + C_L}{C_p}\right)^{3/2} > Z. \tag{5.12}$$

Thus, a small capacitance parallel to the inductance increases the effective characteristic impedance and, in turn, the effective critical voltage.

In order to calculate the height of the dual Shapiro step, we again consider the overdamped regime. Since the exponential factor also influences the time scales of the system, the condition for the overdamped regime is slightly loosened to $\omega_{\mathrm{cl}} \gg e^{-\pi R_Q/4Z}\omega_R$. In this regime, we can again neglect the second-order time derivative and calculate the step height analytically, analogously to Ch. 2. Assuming that $V_{0,\mathrm{dc}} > e^{-\pi R_Q/2Z}V_c$ the first step at the current $I_S = e\omega_0/\pi$ appears at the voltage $V_S = V_c\left[e^{-\pi R_Q/Z} + (\omega_0/\omega_R)^2\right]^{1/2}$. The height of the step at constant current is on the other hand given by

$$\Delta V = \frac{V_{\mathrm{ac}}}{\sqrt{1 + e^{\pi R_Q/Z}\,(\omega_0/\omega_R)^2}}, \tag{5.13}$$

valid to first order in $V_{\mathrm{ac}}/e^{-\pi R_Q/2Z}V_c$. Since there is no qualitative difference between the overdamped system in the ground state approximation and the ideal system in Ch. 2, Figs. 2.4 and 2.5 are still valid for our current system. We only need to make the substitution $V_c \mapsto V_c e^{-\pi R_Q/2Z}$ which results in a renormalization of the RC-time $\omega_R \mapsto \omega_R e^{-\pi R_Q/2Z}$. Additionally, all of the calculations done in Ch. 3 regarding the influence of thermal, resistive noise can also be mapped onto our current system using the same substitutions.

However, for $\omega_{\mathrm{cl}} \leq e^{-\pi R_Q/4Z}\omega_R$, the second-order time derivative in Eq. (5.11) becomes important. While we can not calculate the step height analytically in this regime, we can solve the differential equation numerically in order to better illustrate the dependence of the step height on all relevant parameters. Figure 5.3 displays the height of the first dual Shapiro step as a function of the quality factor and the drive frequency. Here, we can clearly see that the

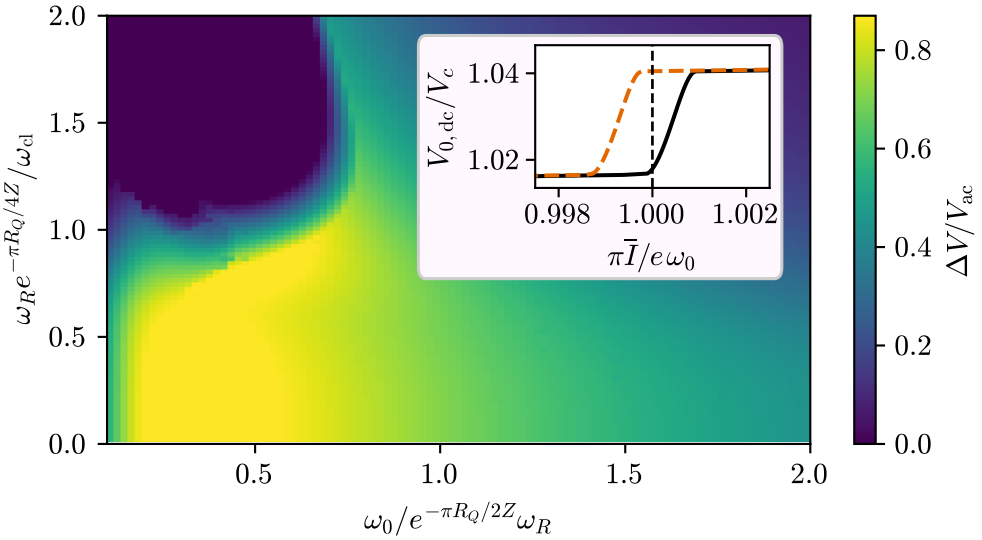

Figure 5.3: Height of the first dual Shapiro step in the ground state approximation as a function of the quality factor and the drive frequency. The figure was obtained by solving Eq. (5.11) numerically for $V_{\rm ac} = 0.1e^{-\pi R_Q/2Z}V_c$. The largest steps appear in the overdamped regime $\omega_{\rm cl} \gg e^{-\pi R_Q/4Z}\omega_R$. The inlay displays how hysteresis can change the position of the dual Shapiro step. The curves were obtained by solving Eq. (5.11) numerically for $\omega_{\rm cl} = 0.5e^{-\pi R_Q/4Z}\omega_R$ and $\omega_0 = e^{-\pi R_Q/2Z}\omega_R$ with two different initial conditions.

maximum step height can only be achieved in the overdamped regime. In the underdamped regime, the step heights becomes smaller and hysteresis begins to occur, making it very unfavorable for a precise measurement of the step position.

One might think that the exponential factor does not influence the maximum possible step height and instead only the drive frequency that we need to apply in order to reach the maximum height. This is not the case for two reasons: First, our theoretical calculations are only valid for $V_{\rm ac} \ll e^{-\pi R_Q/2Z}V_c$ and, as we have discovered in Sec. 2.3, the maximum step height is reached for $V_{\rm ac} \simeq e^{-\pi R_Q/2Z}V_c$. Thus, the optimum drive $V_{\rm ac}$ is reduced by the exponential factor. Since the step height scales with the drive, the effective maximum step height is similarly reduced. Second, going to smaller and smaller drive frequencies in order to reach the maximum possible step height is not experimentally feasible. A smaller drive frequency ω_0 causes the dual Shapiro steps to appear at smaller currents $I_S = e\omega_0/\pi$. Since it is not possible to measure currents far below the nano-amps range [2], the effective maximum step height is reduced.

Modern fabrication techniques allow for on-chip inductances of the order of 500 nH [26, 28, 29]. For our purposes, we would, thus, require a parasitic capac-

itance of the order of 100 fF in order to obtain an impedance $Z = \sqrt{L/C_p}$ of about 3 kΩ. This seems to be an achievable order of magnitude [6] and given the many groups in different fields working on the fabrication of superinductances, we are confident that this limit will be reached soon.

Lastly, we are going to discuss the influence of thermal excitations in the LC-circuit composed of the parasitic capacitance C_p and the superinductance L. If we include thermal excitation of higher energy levels in our ground state approximation, Eq. (5.10) has to be rewritten in terms of the trace with the density operator $\hat{\rho}$ [30] and we obtain

$$\mathrm{Tr}\left\{\hat{\rho}\,\sin\left[\frac{\pi}{e}(\hat{Q}_q + Q_{\mathrm{cl}})\right]\right\} = e^{-\pi R_Q(1+2\bar{n})/2Z}\sin\left(\frac{\pi}{e}Q_{\mathrm{cl}}\right) \tag{5.14}$$

where $\bar{n} = 1/(e^{\hbar\omega_q/k_BT} - 1)$ is the average number of photons in the LC-resonator given by the Bose-Einstein statistic. For a realistic resonance frequency of the order of $\omega_q/2\pi \simeq 1\,\mathrm{GHz}$ and a temperature of $T \simeq 20\,\mathrm{mK}$, we obtain $\bar{n} \simeq 0.1$. Thus, the influence of charge fluctuations in the LC-resonator is negligible.

5.3 Simulation of the quantum system

In order to confirm the results of this chapter, we solve the coupled system between the Hamiltonian in Eq. (4.3) and the equation of motion in Eq. (4.4) numerically. The Schrödinger equation is implemented as follows. The numerical evolution of the quantum mechanical state from time t_k to $t_{k+1} = t_k + \Delta t$ is performed using the Crank-Nickelson method [31] also known as Cayley's expansion of the time-evolution operator $\hat{U}(t_{k+1}, t_k) = e^{-i\Delta t\hat{H}(t_k)/\hbar}$. This method conserves the unity of the time-evolution operator by expanding the exponential function for small Δt using the simple trick

$$e^{-i\Delta t\hat{H}(t_k)/\hbar} = \frac{e^{-i\Delta t\hat{H}(t_k)/2\hbar}}{e^{i\Delta t\hat{H}(t_k)/2\hbar}} = \frac{1 - i\Delta t\hat{H}(t_k)/2\hbar}{1 + i\Delta t\hat{H}(t_k)/2\hbar} + \mathcal{O}\left(\Delta t^3\right). \tag{5.15}$$

Using this approximation, we can perform a time step with $\hat{U}(t_{k+1}, t_k)|\psi(t_k)\rangle = |\psi(t_{k+1})\rangle$. Since the approximation is unitary, the state will remain normalized throughout the entire evolution.

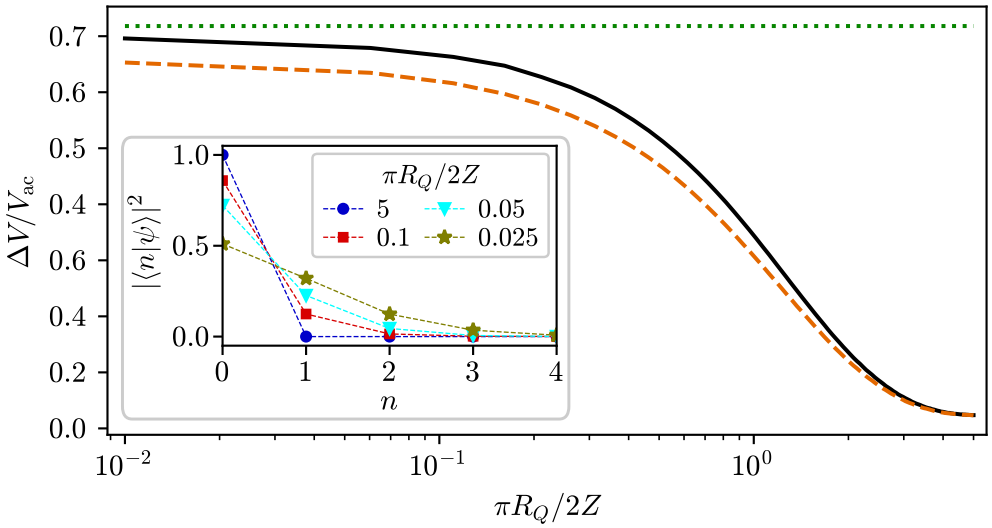

Figure 5.4: Height of the first dual Shapiro step as a function of the characteristic impedance Z for $\omega_{\mathrm{cl}} = 2\omega_R$, $\omega_q = 3\omega_R$, $\omega_0 = 1.1\omega_R$, and $V_{\mathrm{ac}} = 0.1V_c$. The solid, black line displays the result obtained by a numerical calculation of the coupled system in Eqs. (4.3) and (4.4). The dotted, green line shows the numerical solution of Eq. (5.1) valid in the high impedance regime $Z \gg R_Q$. The dashed, orange line represents the numerical result of the ground state approximation in Eq. (5.11). The ground state approximation provides a good, conservative approximation for the results of the quantum simulation, especially for $Z \ll R_Q$. The inlay shows the occupation of the harmonic oscillator states for different values of Z/R_Q. For $Z \gg R_Q$, the higher states become more occupied which leads to a larger discrepancy between the ground state approximation and the full solution.

The Hamiltonian is expressed in the basis of the harmonic oscillator with plasma frequency ω_q. This is useful, since we want to compare the behavior of the full system to the effective equation of motion in the ground state approximation derived in the previous section. For the numerical calculation, however, we have to make sure to include enough states of the harmonic oscillator for the simulation to converge. The chosen representation then allows us to easily check for which parameters the ground state approximation breaks down.

After calculating one time step of the wave function, we need to calculate the expectation value of $\hat{Q}_q/C_p$. To increase numerical accuracy, we use Eq. (5.9) to rewrite the expectation value analogously to the previous section. Next, we use a standard backward Euler method [32] to solve the resulting equation of motion and obtain a value for the classical charge Q_{cl} at time t_{k+1}. This result can then be reinserted into the Hamiltonian to calculate the next step in time.

In Fig. 5.4, we compare the numerical results of the quantum simulation to our numerical solutions of Eqs. (5.1) and (5.11). As expected, we find that the approximation in the high impedance regime provides an upper limit to the quantum simulation, valid for $Z \gg R_Q$. The ground state approximation gives a good, conservative approximation for the height of the step in the quantum simulation, especially for $Z \ll R_Q$. In this regime, the condition for the ground state approximation $\omega_q \gg eV_c/\hbar \simeq \omega_{\mathrm{cl}}\sqrt{Z/R_Q}$ is better fulfilled. This is also evidenced by the occupation of the harmonic oscillator states for different values of Z/R_Q. For $Z \gg R_Q$, the higher states become more occupied which leads to a larger discrepancy between the ground state approximation and the full solution.

Naturally, the simulation of the full system is much more involved and time-consuming than solving the single equation of motion in the ground state approximation. As the approximation works quite well over a wide range of parameters, especially for $Z \lesssim R_Q$, it is often useful to initially calculate the step height and position using the ground state approximation. The obtained results can then be used as initial values for the full simulation to find the step position and height more efficiently.

Chapter 6

Conclusion and Outlook

This thesis has dealt with the topic of dual Shapiro steps in the presence of a superinductance and a parasitic capacitance. In Ch. 2, we have discussed the concept of phase-slip junctions and introduced an idealized circuit for the measurement of dual Shapiro steps. Using this circuit, we have studied the emergence of Bloch oscillations with Bloch frequency $\omega_B = \pi \overline{I}_{\mathrm{dc}}/e$ in a DC-biased phase-slip junction. Additionally, we have shown how phase-locking between the Bloch oscillations and a small AC-drive leads to dual Shapiro steps at constant current in the IV-curve.

The influence of thermal fluctuations on these dual Shapiro steps has been examined in Ch. 3. There, we have first treated the case of classical, resistive noise and discovered that the step height needs to be compared to the temperature scale $k_B T/e$ to determine whether the dual Shapiro steps are being washed out by thermal fluctuations. By extending our analysis to quantum noise, we have learned that even at zero temperature the linewidth of the Bloch oscillation is finite, which renders filtering below this effective temperature of the Bloch oscillations useless.

After studying all these properties in an ideal circuit, we have added the parasitic capacitance as well as the superinductance to the ideal system in order to make it more realistic. In Ch. 4, we have described the resulting circuit by a Schrödinger equation which is coupled to a classical equation of motion. With this, we have finally been able to analyze how the parasitic capacitance and the superinductance influence the dual Shapiro step height in Ch. 5. First, we have focused on the high impedance regime where the characteristic impedance $Z = \sqrt{L/C_p}$ is much larger than the resistance quantum. In this regime, we have calculated the step height perturbatively for a small parasitic capacitance.

We have discovered that such a small capacitance even increases the step height at high impedance. Next, we have taken a closer look at the limit of high plasma frequency $\omega_q \gg \omega_0, eV_c/\hbar$, where the quantum system remains in the ground state and only the classical equation of motion has to be solved. Here, the leading effect of the parasitic capacitance is a reduction of the critical voltage of the phase-slip junction V_c by a factor of $e^{-\pi R_Q/2Z}$. Thus, the effect of the parasitic off-chip capacitance can be remedied by an on-chip inductance, as long as the characteristic impedance Z is of the order of $\pi R_Q/2 \approx 10\,\mathrm{k\Omega}$. In this context, we have also discussed the influence of a small capacitance parallel to the superinductance which slightly increases the effective characteristic impedance. Finally, we have performed numerical simulations to validate the analytical results.

Even though Bloch oscillations in small Josephson junctions have been known for more than 30 years, many open questions still remain to be answered. The most significant appears to be the question about the realization of the superinductance. Recent experiments indicate three promising candidates: Josephson junction arrays [26], nanowires [5], and geometric coils [29]. All implementations offer different advantages and drawbacks and it is not yet clear which one is the most suitable for the observation of Bloch oscillations. Another question related to the experimental implementation that requires further theoretical analysis is finding the optimal filtering. As indicated in Ch. 3, filtering is a necessary ingredient for the measurement of Bloch oscillations. How different filtering schemes effect the washing out of the dual Shapiro steps remains an important question for future research. In addition, Bloch oscillations do not necessarily have to be measured via dual Shapiro steps. They can also be measured dispersively via the frequency shift to the resonance frequency of a microwave readout resonator [6]. We are curious to find out how our results can be adapted to this different measurement setup.

Of course, there are also some smaller questions regarding our theoretical discussion that still need to be answered. For example, how Landau-Zener tunneling or contributions of higher frequency to the periodic band structure influence the height of the dual Shapiro step. Throughout our work we have neglected both influences since Landau-Zener tunneling can be made small by working at small currents and the higher frequency contributions can be reduced by a large ratio of E_J/E_C. Nevertheless, they are still interesting subjects for future research.

Appendix A

Derivation of the phase-slip energy

We want to give a derivation of the semi-classical approximation of the phase-slip energy E_S which corresponds to the bandwidth of the lowest energy band of a Josephson junction with Josephson energy E_J and capacitance C. This Josephson junction can be described by the Hamiltonian

$$\hat{H} = \hat{T} + \hat{V} = 4E_C\,\hat{n}^2 + E_J\left[1 - \cos\left(\hat{\varphi}\right)\right], \tag{A.1}$$

which we already derived in Sec. 2.1[1]. In order to simplify the following calculations, we have introduced the normalized operators $\hat{n} = \hat{q}/2e$ and $\hat{\varphi} = 2\pi\hat{\phi}/\Phi_0$, with $[\hat{n}, \hat{\varphi}] = i$. The bandwidth of the lowest energy band can be approximated by the tunneling amplitude between two adjacent minima of the cosine potential. Using the well-known WKB-approximation to the tunneling amplitude [33], we obtain

$$E_S \simeq \hbar\omega e^{iS}, \tag{A.2}$$

where ω is the attempt frequency and S the tunneling action. The attempt frequency can be approximated by the oscillation frequency of the flux around a minimum of the cosine potential. For this reason, we expand the cosine potential up to second order for small φ

$$\hat{H} = 4E_C\hat{n}^2 + \frac{E_J}{2}\hat{\varphi}^2 \tag{A.3}$$

and, thus, obtain the Hamiltonian of a harmonic oscillator with oscillation frequency $\omega = \sqrt{8E_CE_J}/\hbar$.

[1] Note that the external current source is not important for the calculation of the phase-slip energy and we have, therefore, set $Q = 0$.

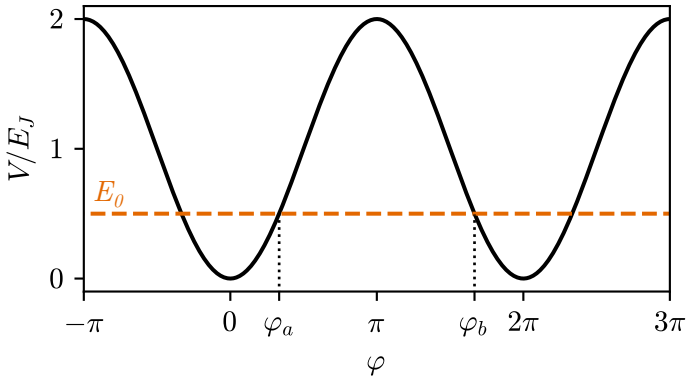

Figure A.1: Periodic Josephson potential as a function of the normalized node flux $\varphi = 2\pi\phi/\Phi_0$ (black, solid). The orange, dashed line indicates an exemplary ground state energy with the classical turning points φ_a and φ_b.

Next, we calculate the semi-classical tunneling action given by an integral of the classical momentum — in our case the normalized charge $n(\varphi)$ — over the classically forbidden tunneling region from φ_a to φ_b, as displayed in Fig. A.1. We obtain

$$S = \int_{\varphi_a}^{\varphi_b} d\varphi\, n(\varphi) = i \int_{\varphi_a}^{\varphi_b} d\varphi \sqrt{\left[V(\varphi) - E_0\right]/4E_C} \equiv iS_0, \tag{A.4}$$

with $V(\varphi) = E_J[1 - \cos(\varphi)]$ and $E_0 = \hbar\omega/2$ the ground state energy of the harmonic approximation in Eq. (A.3). Here, S_0 can be interpreted as the semi-classical action of the tunneling trajectory obtained by mirroring the potential in Fig. A.1 on the axis of the ground state energy. As a rough approximation, we can assume $E_0 = 0$ and consequently set the classical turning points $\varphi_a = 0$, $\varphi_b = 2\pi$. This leads to a tunneling action of the form

$$S_0 = \int_0^{2\pi} d\varphi \underbrace{\sqrt{E_J\left[1 - \cos(\varphi)\right]/4E_C}}_{\sqrt{E_J/2E_C}\sin(\varphi/2)} = \sqrt{8E_J/E_C}. \tag{A.5}$$

Together with the previously calculated oscillation frequency, we, thus, obtain the 0^{th} order result valid to exponential accuracy

$$E_S \simeq \sqrt{E_C E_J} e^{-\sqrt{8E_J/E_C}}. \tag{A.6}$$

To improve our approximation, we can take into account the ground state energy $E_0 = \sqrt{2E_C E_J}$. The integral boundaries can be approximated by the turning points of the harmonic oscillator in Eq. (A.3). We obtain $\varphi_a = \sqrt{2E_0/E_J}$ and

$\varphi_b = 2\pi - \varphi_a$. This leads to a correction of the tunneling action of the form [34]

$$\begin{aligned}\Delta S_0 &= \int_{\varphi_a}^{\pi} d\varphi \sqrt{\left[V(\varphi) - E_0\right]/E_C} - \int_0^{\pi} d\varphi \sqrt{V(\varphi)/E_C} \\ &= -\int_0^{\varphi_a} d\varphi \sqrt{V(\varphi)/E_C} - E_0 \int_{\varphi_a}^{\pi} d\varphi \Big(\sqrt{E_C[V(\varphi) - E_0]} + \sqrt{E_C V(\varphi)}\Big)^{-1}.\end{aligned} \tag{A.7}$$

This integral can be simplified if we assume the ground state energy E_0 to be small compared to the potential barrier E_J. In this regime, we can neglect terms of the order $\mathcal{O}(\sqrt{E_0/E_J})$ and approximate $\sin(\varphi_a/2) \simeq \sqrt{E_0/2E_J}$. We, thus, obtain

$$\begin{aligned}\Delta S_0 &\simeq -\int_0^{\varphi_a} d\varphi \sqrt{E_J/2E_C}\varphi - E_0 \int_{\varphi_a}^{\pi} d\varphi \Big(2\sqrt{E_C V(\varphi)} - \sqrt{E_C} E_0/2\sqrt{V(\varphi)}\Big)^{-1} \\ &\simeq -\int_{\varphi_a}^{\pi} d\varphi \underbrace{\frac{1}{2}\sin^{-1}\left(\frac{\varphi}{2}\right)}_{\simeq 1/\varphi} \\ &\simeq \frac{1}{4}\ln\left(\frac{E_C}{E_J}\right),\end{aligned} \tag{A.8}$$

where we additionally neglected any constant terms which do not contribute to the scaling of the phase-slip energy with E_C and E_J. As a final result for the phase-slip energy, we find

$$E_S \simeq \sqrt{E_C E_J}\left(\frac{E_J}{E_C}\right)^{1/4} e^{-\sqrt{8E_J/E_C}} = E_C^{1/4} E_J^{3/4} e^{-\sqrt{8E_J/E_C}}. \tag{A.9}$$

The same result can also be obtained via wave function matching with quadratic connection formulas for a barrier as explained in Ref. [35]. Our result shows that the band gap scales exponentially with $\sqrt{E_J/E_C}$. Consequently, a large parasitic capacitance decreases the phase-slip energy and, thus, the amplitude of the Bloch oscillations exponentially, see Ch. 4.

Acknowledgements

Last but not least, I would like to thank all the people without whom this last year would certainly not have been the same. First of all, I would like to thank my supervisor, Fabian Hassler. Without him this work would not have been possible. I am grateful for countless fruitful discussions, whether they were related to the work on this thesis or simply interesting physics. His support and enthusiasm have been a constant source of motivation and inspiration.

Second, I want to thank Johannes Fink and Matilda Peruzzo for an insightful look at the experimental perspective and a great week in Vienna.

In addition, I want to thank my office mates Uta Meyer, Marco Roth and Daniel Otten for always finding the time for some helpful remarks. I also want to thank Martin Rymarz for interesting, entertaining discussions and making sure the light in our office was turned on. Then, I want to thank Lucia Gonzalez for making the DPG conference more fun and for always having an open ear for me.

I want to thank all present and former members of the IQI. I want to thank David DiVincenzo for the welcoming and relaxed atmosphere at the institute and Helene Barton who has made all the bureaucracy seem so easy.

Finally, I want to thank my parents and my partner René for all their support and for being there every step of the way.

Bibliography

[1] D.V. Averin, A.B. Zorin, and K.K. Likharev. *Bloch oscillations in small Josephson junctions.* Sov. Phys. JETP **61**, 407 (1985).

[2] J. P. Pekola, O.-P. Saira, V. F. Maisi, A. Kemppinen, M. Möttönen, Y. A. Pashkin, and D. V. Averin. *Single-electron current sources: Towards a refined definition of ampere.* Rev. Mod. Phys. **85**, 1421 (2013).

[3] J. E. Mooij and Yu. V. Nazarov. *Superconducting nanowires as quantum phase-slip junctions.* Nature Phys. **2**, 169 (2006).

[4] L. S. Kuzmin and D. B. Haviland. *Observation of the Bloch oscillations in an ultrasmall Josephson junction.* Phys. Rev. Lett. **67**, 2890 (1991).

[5] J. S. Lehtinen, K. Zakharov, and K. Yu. Arutyunov. *Coulomb blockade and Bloch oscillations in superconducting Ti nanowires.* Phys. Rev. Lett. **109**, 187001 (2012).

[6] V. E. Manucharyan. *Superinductance.* PhD thesis, Yale University (2012).

[7] A. D. Marco, F. W. J. Hekking, and G. Rastelli. *Quantum phase-slip junction under microwave irradiation.* Phys. Rev. B **91**, 184512 (2015).

[8] J. Ulrich and F. Hassler. *Dual approach to circuit quantization using loop charges.* Phys. Rev. B **94**, 094505 (2016).

[9] S. Shapiro. *Josephson currents in superconducting tunneling: The effect of microwaves and other observations.* Phys. Rev. Lett. **11**, 80 (1963).

[10] W. H. Parker, B. N. Taylor, and D. N. Langenberg. *Measurement of $\frac{2e}{h}$ using the ac Josephson effect and its implications for quantum electrodynamics.* Phys. Rev. Lett. **18**, 287 (1967).

[11] J. R. Rubbmark, M. M. Kash, M. G. Littman, and D. Kleppner. *Dynamical effects at avoided level crossings: A study of the Landau-Zener effect using Rydberg atoms.* Phys. Rev. A **23**, 3107 (1981).

[12] L. Arndt. *Time-Scales of Charge Relaxation in a Superconducting Island via an Inductive Shunt.* B.Sc. thesis, RWTH Aachen University (2015).

[13] H. Grabert and M. H. Devoret. *Single charge tunneling: Coulomb blockade phenomena in nanostructures.* Springer US, New York (1992).

[14] D.V. Averin, A.B. Zorin, and K.K. Likharev. *Coulomb blockade of single-electron tunneling, and coherent oscillations in small tunnel junctions.* J. Low Temp. Phys. **62**, 345 (1986).

[15] K. K. Likharev. *Dynamics of Josephson junctions and circuits.* Gordon and Breach Publishers (1986).

[16] S. Corlevi, W. Guichard, F. W. J. Hekking, and D. B. Haviland. *Coulomb blockade of Cooper pair tunneling and parity effects in the Cooper pair transistor.* Phys. Rev. B **74**, 224505 (2006).

[17] J. B. Johnson. *Thermal agitation of electricity in conductors.* Phys. Rev. **32**, 97 (1928).

[18] H. Nyquist. *Thermal agitation of electricity in conductors.* Phys. Rev. **32**, 110 (1928).

[19] D. Abbott, B. R. Davis, N. J. Phillips, and K. Eshraghian. *Simple derivation of the thermal noise formula using window-limited Fourier transforms and other conundrums.* IEEE Trans. Educ. **39**, 1 (1996).

[20] D. B. Haviland, L. S. Kuzmin, P. Delsing, and T. Claeson. *Observation of the Coulomb blockade of Cooper pair tunnelling in single Josephson junctions.* Europhys. Lett. **16**, 103 (1991).

[21] D. B. Haviland, Y. Harada, P. Delsing, C. D. Chen, and T. Claeson. *Observation of the resonant tunneling of Cooper pairs.* Phys. Rev. Lett. **73**, 1541 (1994).

[22] Yu. V. Nazarov and Ya. M. Blanter. *Quantum transport: Introduction to nanoscience.* Cambridge University Press, Cambridge (2009).

[23] A. M. Hriscu and Yu. V. Nazarov. *Quantum synchronization of conjugated variables in a superconducting device leads to the fundamental resistance quantization.* Phys. Rev. Lett. **110**, 097002 (2013).

[24] J. Koch, V. Manucharyan, M. H. Devoret, and L. I. Glazman. *Charging effects in the inductively shunted Josephson junction.* Phys. Rev. Lett. **103**, 217004 (2009).

[25] V. E. Manucharyan, J. Koch, L. Glazman, and M. Devoret. *Fluxonium: Single Cooper pair circuit free of charge offsets.*

[26] N. A. Masluk, I. M. Pop, A. Kamal, Z. K. Minev, and M. H. Devoret. *Implementation of low-loss superinductances for quantum circuits.* Phys. Rev. Lett. **109**, 137002 (2012).

[27] L. Arndt, A. Roy, and F. Hassler. *Dual Shapiro steps of a phase-slip junction in the presence of a parasitic capacitance.* arXiv:1802.08123 (2018).

[28] M. T. Bell, I. A. Sadovskyy, L. B. Ioffe, A. Yu. Kitaev, and M. E. Gershenson. *Quantum superinductor with tunable nonlinearity.* Phys. Rev. Lett. **109**, 137003 (2012).

[29] J. M. Fink, M. Kalaee, A. Pitanti, R. Norte, L. Heinzle, M. Davanco, K. Srinivasan, and O. Painter. *Quantum electromechanics on Ssilicon nitride nanomembranes.* Nature Commun. **7**, 12396 (2016).

[30] A. Polkovnikov. *Phase space representation of quantum dynamics.* Ann. Phys. **325**, 1790 (2010).

[31] J. Crank and P. Nicolson. *A practical method for numerical evaluation of solutions of partial differential equations of the heat-conduction type.* Proc. Camb. Phil. Soc. **43**, 50 (1947), reprinted in Advances in Computational Mathematics **6**, 207 (1996).

[32] J. C. Butcher. *Numerical methods for ordinary differential equations.* John Wiley & Sons, New York (2003).

[33] L. D. Landau and E. M. Lifshitz. *Quantum mechanics*, volume 3 of *Course of theoretical physics.* Pergamon Press, London (1958).

[34] Private conversation with F. Hassler.

[35] J. N. L. Connor, T. Uzer, R. A. Marcus, and A. D. Smith. *Eigenvalues of the Schrödinger equation for a periodic potential with nonperiodic boundary conditions: A uniform semiclassical analysis.* J. Chem. Phys. **80**, 5095 (1984).